RSC Advances

ROYAL SOCIETY OF CHEMISTRY

www.rsc.org/advances

RSC Advances

An Experimental and Quantum Chemical Study on the Non-covalent Interactions of a Cyclometallated Rh(III) Complex with DNA and BSA

Roya Esteghamat-Panah,[a] Hossein Farrokhpour,*[a] Hassan Hadadzadeh,*[a] Fatemeh Abyar,[b] and Hadi Amiri Rudbari[c]

[a] *Department of Chemistry, Isfahan University of Technology, Isfahan 84156-83111, Iran*

[b] *Department of Engineering, Ardakan University, Ardakan 89518-95491, Iran*

[c] *Faculty of Chemistry, University of Isfahan, Isfahan 81746-73441, Iran*

Number of Pages: 58

Number of Schemes: 2

Number of Tables: 3

Number of Figures: 16

***Corresponding authors,**

Hassan Hadadzadeh

Professor of Inorganic and Bioinorganic Chemistry

Department of Chemistry, Isfahan University of Technology, Isfahan 84156-83111, Iran

E-mail address: hadad@cc.iut.ac.ir

Hossein Farrokhpour

Associate Professor of Physical Chemistry

Department of Chemistry, Isfahan University of Technology, Isfahan 84156-83111, Iran

E-mail address: h-farrokh@cc.iut.ac.ir

Crystallographic data for [Rh(phpy-κ^2N,C$^{2'}$)$_2$(dafone)]PF$_6$ have been deposited with the Cambridge Crystallographic Data Centre, CCDC 1057307.

RSC Advances

An Experimental and Quantum Chemical Study on the Non-covalent Interactions of a Cyclometallated Rh(III) Complex with DNA and BSA

Roya Esteghamat-Panah,[a] Hossein Farrokhpour,*[a] Hassan Hadadzadeh,*[a] Fatemeh Abyar,[b] and Hadi Amiri Rudbari[c]

[a] *Department of Chemistry, Isfahan University of Technology, Isfahan 84156-83111, Iran*

[b] *Department of Engineering, Ardakan University, Ardakan 89518-95491, Iran*

[c] *Faculty of Chemistry, University of Isfahan, Isfahan 81746-73441, Iran*

Abstract

The interaction of a new cyclometallated Rh(III) complex, $[Rh(phpy\text{-}\kappa^2N,C^{2'})_2(dafone)]^+$ (phpy-$\kappa^2N,C^{2'}$ = pyridine-2-yl-2-phenyl and dafone = 4,5-diazafluoren-9-one), with DNA and BSA was investigated. The *in vitro* cytotoxicity tests of the complex against three cancer cell lines demonstrate that the complex can be introduced as an efficient anticancer agent. The binding of the complex to DNA and BSA was modeled by molecular docking. The three-layer ONIOM method (QM:QM:MM) was employed to calculate the interaction energy between DNA and the complex, where QM and MM are abbreviations of quantum mechanics and molecular mechanics, respectively. The complex and a part of DNA were considered in the QM region at the same theoretical level, whereas the different basis sets for DNA, the complex, and the rest of system were considered in the MM region. The density functional theory (DFT) employing M062X functional was used for the QM parts of the system. M062X functional is one the best DFT functionals, introduced in recent years, which considers the non-covalent interactions properly. The UV spectra of the complex interacting with DNA in the gas phase and water were calculated using two- and three-layer ONIOM method employing time-dependent density functional theory (TD-DFT) to investigate the effect of

the interaction on the electronic structure of the complex. The calculations interestingly confirm the variations observed in the recorded spectra of the complex due to its interaction with DNA.

Introduction

For more than one century, inorganic compounds have been used as anticancer drugs and systematic investigation of their cytotoxic activity began about 75 years ago.[1] The intense studies of the antitumor activity of inorganic and organometallic compounds started after the identification of *cis*-$[PtCl_2(NH_3)_2]$ as an efficient anticancer drug in 1969.[2] Despite the clinical success of *cis*platin, it has the problems such as the cellular acquired resistance and high toxicity,[3] that have led to the consideration of anticancer properties of new complexes containing metals other than platinum.[4,5] Recently, rhodium complexes have been employed in the improvement of metal-based drugs in cancer chemotherapy.[6] Although rhodium is not a bio-essential metal but some rhodium complexes have useful applications in the biological field and through their interaction with DNA, they have considerable pharmacological effects.[7] Organometallic complexes due to their characteristics such as diverse structural types, varied ligand bonding modes, and physico-chemical properties somewhat intermediate between traditional coordination compounds and organic molecules, have great potential application as anticancer drugs[8] and disease therapy.[9] The cyclometallated complexes with C,N-donor ligands have attracted an increasing interest. Since one of the problems of using non-symmetric bidentate ligands is their varied created isomers and (C^N) cyclometallating ligands have tendency to bind with the nitrogen in the axial position, so the number of possible isomers is reduced.[10] 2-phenylpyridine (ppy) is a C,N-donor ligand that its cyclometallated complexes of group 9 have great photochemical and photophysical properties,[11] thus they are used as phosphors in organic light emitting diodes (OLEDs)[12] and

as luminescent labels for biomolecules.[13] Ortho-metallation in these complexes leads to higher energy d–d^* transitions and lower energy metal-to-ligand charge transfer states, that can be attributed to the σ-donor/π-acceptor properties of 2-phenylpyridine ligand.[10] Bioorganometallic chemistry is a new aspect of metal–carbon bond compound reactivity that is about the reactions of organometallic complexes with biological substrates in aqueous solution.[14] Since DNA is the main target of many anticancer compounds,[15] the interaction of rhodium complexes with the double helix DNA has been studied. Anticancer activity of rhodium complexes can be due to their interaction with DNA. It has been seen that rhodium(I), rhodium(II), and rhodium(III) complexes have biological activity.[16] Rhodium(III) complexes with polypyridyl ligands can react with DNA through intercalation of these ligands or *via* formation of Rh–N bonds with cytosine or guanine bases of DNA.[1,16] A number of rhodium(III) complexes such as $[RhCl_3(N–N)(DMSO)]$ (N–N = phen, bpy, dpphen, 1,10-phenanthroline-5,6-dione, dmbpy),[1] $[RhCl_3(Him)(DMSO)_2]$ (Him = imidazole), and $[RhCl_3(NH_3)(DMSO)_2]$[16] show high anticancer activity. Rhodium(II) carboxylato complex, $[Rh_2(\mu\text{-}OOCR)_2(N–N)_2(H_2O)_2](RCOO)_2$ (R = alkyl, hydroxyalkyl, aminoalkyl, N–N = bpy, phen and their derivatives), was found to be active against oral carcinoma, P388 and L1210 leukemia.[16] Dirhodium(II) tetracarboxylate complexes, $Rh_2(\mu\text{-}O_2CR)_4$ (R = Me, Et, Pr, and Bu), exhibit carcinostatic activity against Ehrlich ascites and leukemia L1210 tumors.[17] The dirhodium complexes possessing aromatic ligands, such as *cis*-$[Rh_2(\mu\text{-}O_2CCH_3)_2(dppn)(L)]^{2+}$, where dppn = benzo[i]dipyrido[3,2-*a*:2',3'-c]phenazine, and L = bpy (2,2'-bipyridine), and phen (1,10-phenanthroline), interact with DNA through intercalation.[18] Also, two cationic complexes, $[Rh_2(\mu\text{-}OAc)_2(\eta^1\text{-}OAc)(dppz)(CH_3OH)]^+$ and $[Rh_2(\mu\text{-}OAc)_2(\eta^1\text{-}OAc)(dppn)(CH_3OH)]^+$ (dppz = dipyrido[3,2-*a*:2',3'-*c*]phenazine, and dppn = benzodipyrido[3,2-*a*:2',3'-*c*]phenazine), have cytostatic activity against human skin fibroblast Hs-27.[2]

Until now, few studies of the interaction of cyclometallated Rh(III) complexes with DNA and BSA have been reported, *e.g.*, a cyclometallated Rh(III) complex, $[Rh(ppy)_2(phi)]^+$, has been shown to be effective in binding DNA by inserting the 9,10-phenanthrene quinone diimine (phi) moiety between the base pairs in the DNA duplex;[10] an organorhodium complex of $[(\eta^5\text{-}C_5Me_5)RhCl(L)]$ (L = benzylidene(4-*tert*-butylphenyl) amine 4-methyl ester) binds to DNA through the intercalative/electrostatic interactions and exhibits better cytotoxicity against the human lung cancer cell line (A549) than *cis*platin;[19] and three cyclometallated Rh(III) complexes, $[Rh(2\text{-}C_6H_4py)_2(L)]$ (LH = 4-MePipzcdtH, MorphcdtH, and 4-BzPipercdtH), bind to CT-DNA *via* an intercalative mode.[7]

In the present study, we have synthesized a new cyclometallated Rh(III) complex, $[Rh(phpy\text{-}\kappa^2N,C^{2'})_2(dafone)]PF_6$, with pyridine-2-yl-2-phenyl (phpy-$\kappa^2N,C^{2'}$) and 4,5-diazafluoren-9-one (dafone) ligands. The complex was characterized by elemental analysis, spectroscopic methods, and X-ray crystallography. The potential of its interaction with DNA and antiproliferative behavior of this complex have been examined. Several techniques including electronic absorption titration, fluorescence spectroscopy, and viscosity measurement have been employed to monitor its prospective interaction with fish sperm DNA (FS-DNA). Also, UV–Vis and fluorescence spectroscopy have been used to evaluate the binding behavior of the complex to bovine serum albumin (BSA). Furthermore, its cytotoxicity towards three human cancer cell lines, *viz.,* hepatocellular liver carcinoma (HepG2), colorectal adenocarcinoma (HT-29), and neuroblastoma carcinoma (SH-SY5Y), has been evaluated using the MTT colorimetric assay. Finally, the molecular docking, two-layers (QM/QM), and three-layers (QM/QM/MM) calculations were performed to obtain detailed binding information of the Rh(III) complex with DNA in the gas phase and water. In addition, the experimental UV spectra of the Rh(III) complex before and after interaction with DNA have been compared with its calculated UV spectra.

Experimental section

Materials and methods

The starting material, $[Rh(phpy\text{-}\kappa^2N,C^{2'})_2Cl]_2$, was prepared according to the literature.[20] All chemicals and solvents were of high purity Merck compounds and used without any further purification. $RhCl_3 \cdot 3H_2O$, Tris(hydroxymethyl)-aminomethane (Tris) buffer, and ethidium bromide (3,8-diamino-5-ethyl-6-phenylphenanthridinium bromide, EthBr) were of analytical reagent grade and obtained from Merck. Double-stranded fish sperm deoxyribonucleic acid (ds-FS-DNA), bovine serum albumin (BSA), 3-(4,5-dimethylthiazole-2-yl)-2,5-diphenyl tetrazolium bromide (MTT), and RPMI 1640 culture medium were purchased from Sigma–Aldrich. Doubly distilled deionized water was used for preparing all solutions for DNA- and BSA-binding studies.

Elemental analysis (C, H, and N) was performed by a Heraeus CHN-O-Rapid elemental analyzer. Fourier-transform infrared spectra were recorded in the solid state (KBr disks) on an FT-IR JASCO 680-PLUS spectrometer in the region of 4000–400 cm^{-1}. Electronic absorption spectra were taken with a UV-JASCO-570 spectrophotometer using quartz cells with a path length of 10 mm. Luminescence measurements were performed on a Shimadzu corporation Chart 200–91527 spectrofluorimeter. ^1H NMR data were obtained by a Bruker DRX-400 MHz Avance spectrometer at ambient temperature in DMSO-d_6 with tetramethylsilane (TMS; δ = 0 ppm) as the internal standard. Viscometric titrations were carried out using an Ubbelohde viscometer maintained at a constant temperature of 298.0(±0.1) K in a thermostatic water bath.

Synthesis of $[Rh(phpy\text{-}\kappa^2N,C^{2'})_2(dafone)]PF_6$

The synthetic route to [Rh(phpy-$\kappa^2N,C^{2'}$)$_2$(dafone)]PF_6 is shown in Scheme 1. A mixture of [Rh(phpy-$\kappa^2N,C^{2'}$)$_2$Cl]$_2$ (223 mg, 0.25 mmol) and 4,5-diazafluoren-9-one (118.3 mg, 0.65 mmol) was added to EtOH/$CHCl_3$ (2:1 v/v), stirred and refluxed for 7 h. The yellow solution was slowly evaporated to dryness. The light brown solid, [Rh(phpy-$\kappa^2N,C^{2'}$)$_2$(dafone)]Cl, was dissolved in water (10 mL) and precipitated from solution as a hexafluorophosphate salt by the addition of an excess amount of NH_4PF_6. The final product, [Rh(phpy-$\kappa^2N,C^{2'}$)$_2$(dafone)]PF_6, was collected by suction filtration, rinsed with cold water and diethylether, and then air dried. For further purification, the yellow precipitate was recrystallized by slow diffusion of diethylether into a saturated solution of the complex in CH_3CN. After 1 week at room temperature, light brown single crystals of [Rh(phpy-$\kappa^2N,C^{2'}$)$_2$(dafone)]PF_6 suitable for X-ray crystallography were formed in a 83% yield. Anal. Calcd for $C_{33}H_{22}F_6N_4O_2PRh$: C, 52.54; H, 2.94; N, 7.43. Found: C, 52.30; H, 3.08; N, 7.55%. ^{1}H NMR (DMSO-d_6, 400 MHz): δ/ppm 6.27 (d, 2H), 6.98 (t, 2H), 7.10 (t, 2H), 7.27 (t, 2H), 7.71 (dd, 2H), 7.81 (d, 2H), 7.87 (d, 2H), 7.97 (d, 2H), 8.07 (dd, 2H), 8.30 (d, 2H), 8.41 (d, 2H). IR (KBr disc): ν_{max}/cm^{-1} 843 (PF_6^-) and 1739 (C=O). UV–Vis: λ_{max} (CH_3CN)/nm (ε/M^{-1} cm^{-1}) 359 (12800), 296 (39000), 259 (61000), 239 (134200).

Crystal structure determination

The crystal structure of [Rh(phpy-$\kappa^2N,C^{2'}$)$_2$(dafone)]PF_6 was obtained by the single crystal X-ray diffraction technique. The X-ray diffraction measurement of the complex was performed on a Bruker–Nonius X8 ApexII diffractometer equipped with a CCD area detector using graphite-monochromated Mo $K\alpha$ radiation (λ = 0.71073 Å) at 298(2) K. Data were collected and reduced by multiscan method with the Bruker software.[21] The structure was solved by the direct method[22] and then developed by a least-squares refinement on F^2 using SHELXL in an anisotropic (for non-hydrogen atoms) approximation.[23] All the hydrogen

atoms were placed at the calculated positions and constrained to ride on their parent atoms. The complete conditions of the data collection and structure are given in Table S1 (ESI†)

DNA binding experiments

The DNA binding experiment with the complex was carried out in the buffer solution (5 mM Tris–HCl/10 mM NaCl, pH = 7.2) that was prepared using double-distilled deionized water. The solubility of the complex as hexafluorophosphate salt, [Rh(phpy-$\kappa^2N,C^{2'}$)$_2$(dafone)]PF_6, was not enough in the buffer solution (aqueous medium). For DNA and BSA interaction studies, the purified [Rh(phpy-$\kappa^2N,C^{2'}$)$_2$(dafone)]PF_6 complex was then exchanged to its perchlorate (ClO_4^-) salt by precipitating a solution of the complex in acetone/acetonitrile with tetrabutylammonium perchlorate. The orange precipitate, [Rh(phpy-$\kappa^2N,C^{2'}$)$_2$(dafone)]ClO_4, was collected by filtration, washed with cold acetone and then air dried.

Caution*: Salts of perchlorate and their metal complexes are potentially explosive and should be handled with great care and in small quantities.*

The elemental analysis of the perchlorate salt of the complex was completely consistent with the proposed molecular formula. A stock solution of [Rh(phpy-$\kappa^2N,C^{2'}$)$_2$(dafone)]ClO_4 was prepared by dissolving of it in an aqueous solution, and then diluted suitably with the corresponding buffer to the required concentration. A stock solution of ds-FS-DNA was prepared by dissolving the desired amount of DNA in the Tris–HCl/NaCl buffer solution and stored at 4 ^oC in the dark and used after no more than 4 days. The FS-DNA concentration (moles of bases per liter) was determined spectroscopically using the molar extinction coefficient at the maximum of the long-wavelength absorbance (ε_{260} = 6600 dm^3 $mole^{-1}$ cm^{-1}). The ratio of the UV absorbance at 260 and 280 nm (A_{260}/A_{280}) was *ca.* 1.8, indicating that the DNA solution was sufficiently protein-free.[24] The UV–Vis spectral feature of [Rh(phpy-$\kappa^2N,C^{2'}$)$_2$(dafone)]ClO_4 did not change on keeping its buffered solution for 48 h and no

precipitation was seen even after long storage at room temperature (at least 3 weeks after preparation), which indicates stability of the Rh(III) complex.

The absorption titration experiment of the Rh(III) complex in buffer solution was performed at a fixed concentration of the complex (2×10^{-5} M), while varying the concentration of DNA. Absorbance values were recorded after each successive addition of the DNA solution and incubation (*ca.* 5 min). The intrinsic binding constant, K_b, of the complex with FS-DNA was acquired by monitoring the changes in the ligand-based absorbance band of 303 nm, with increasing concentration of DNA at 25°C.

The binding specificity of the Rh(III) complex with FS-DNA was also studied by the fluorescence titration method. The competitive binding study involves the addition of the complex to FS-DNA pretreated with EthBr ([FS-DNA]/[EthBr] = 100), and the measurement of the resulting emission intensity. A DNA solution (1.3×10^{-4} M) was pretreated with ethidium bromide (1.3×10^{-6} M) at a saturating binding level. Before measurements, the mixture was shaken up and incubated at room temperature for 30 min. Then the DNA–EthBr solution was excited at 520 nm and the emission intensity of this system upon addition of increasing amounts of the complex to a fixed concentration of the DNA–EthBr system, was measured in the range of 535–750 nm.

In viscosity measurement, fish sperm DNA sample solution was prepared by sonication to minimize complexities arising from DNA flexibility.[25] In this experiment, Double-stranded fish sperm DNA (1 mM), buffer solution (5 mM Tris–HCl/50 mM NaCl at pH 7.2) and increasing concentrations of the Rh(III) complex were used. The DNA–complex mixture was incubated for 5 min at room temperature after each addition of the complex, to complete the interaction between DNA and the complex. The flow times were measured with a digital stopwatch. Each sample was measured three times, and an average flow time was calculated The data are presented as $(\eta/\eta_0)^{1/3}$ *vs.* R (= [Complex]/[DNA]), where η is the viscosity of the

DNA solution in the presence of the complex, and η_0 is that of the DNA solution alone. The viscosity values were calculated from the observed flow time of the DNA-containing solutions (t) corrected for that of the buffer alone (t_0), $\eta = (t - t_0)/t_0$.[26]

BSA binding experiments

A stock solution of BSA (3.2×10^{-4} M) was prepared in Tris–HCl buffer (5 mM, pH 7.2) and stored in the dark at 4 °C for further use. The absorption titration experiment was carried out by keeping the concentration of BSA constant while varying the concentration of the Rh(III) complex. The changes in the absorption spectrum of BSA (2.5 mL solution, containing 6×10^{-6} M BSA) were recorded in the range of 200–400 nm after each successive addition of the stock solution of the Rh(III) complex (5×10^{-4} M) and equilibration (*ca.* 5 min) at room temperature.

The fluorescence emission spectra were observed between 308 and 550 nm by varying the concentration of the Rh(III) complex with the excited BSA at 290 nm. In this experiment, the emission intensity of BSA was recorded after each successive addition of the stock solution of the Rh(III) complex (5×10^{-4} M) to a fixed concentration of BSA (2.5 mL solution, containing 6×10^{-6} M BSA). Each sample was allowed to equilibrate for 5 min after each addition at room temperature. The inner–filter effect was also taken into account, but it was not found so significant effect on the measurements.

Cell culture

The HepG2 liver cancer, HT-29 colon cancer, and SH-SY5Y neuroblastoma cancer cell lines were obtained from the cell bank of Pasteur Institute of Iran. The cells were routinely grown in an RPMI 1640 medium containing 10% (v/v) heat inactive fetal bovine serum (Gibco), glutamine (2 mM), and 1% penicillin and streptomycin (Invitrogen) in a highly humidified atmosphere (95% air and 5% CO_2 at 37°C).

Cytotoxicity assay

For evaluation of growth inhibition tests, the cells were seeded in 96-well plates (at density of 5×10^3 cells/well). A stock solution of the Rh(III) complex (as a perchlorate salt) (10^{-2} M) was prepared by dissolving it in DMSO. It was then diluted in RPMI medium and added to the wells to obtain the final concentrations (0.5–40 μM). After 24 h incubation at 37°C, the MTT solution (20 μL, 0.5 mg mL^{-1}, Sigma) was added to each well, and the plates were incubated again for 4 h at 37°C. The viable cells react with MTT to form purple formazan crystals. Then, the medium was exchanged with DMSO (200 μL) to dissolve formazan crystals. The cells were incubated and protected from light for 20 min at room temperature. The absorbance of each well was measured at 545 nm using an ELISA reader (Bio-Tek, Elx 808, Germany) and compared to the values of the control cells incubated without the complex. The IC_{50} values (the drug concentration causing 50% reduction in cellular viability) were determined by plotting the percentage inhibition against the drug concentration on a logarithmic graph.

Theoretical section

Molecular docking

The molecular docking analysis of the Rh(III) complex with DNA and BSA were carried out using Hex 6.1 software.[27] The structure of DNA (PDB ID: 423D) with sequence d $(ACCGACGTCGGT)_2$ and BSA (PDB ID: 4F5S) were taken from the protein data bank (PDB)[28] (RCSB) with the resolution of 1.60 and 2.47 Å, respectively. The structure of the complex was taken from its X-ray crystallography data. It should be mentioned that the structures of DNA, BSA, and the complex were considered rigid during the docking calculations. Hex 6.1 is the only docking and superposition program which performs docking calculations employing Spherical Polar Fourier (SFP) Correlations to accelerate the

calculations and it is still one of a few docking programs which has built-in graphics to view the results.[29] The parameters selected for docking process *via* the Hex software are: correlation type shape only, FFT mode at 6D level, grid dimension of 6 with receptor range 180, ligand range 180 with twist range 360, distance range 40, and solution 2000. The size of the grid map was set to 96 × 96 × 96 Å^3 with a grid-point spacing of 0.60 Å in the *x*, *y*, and *z* directions, respectively. For the detection of the possible binding sites by scanning the entire surface of the target (DNA and BSA) and finding a location with the highest binding affinity, the blind docking (BD) process was used.[30,31] For the docking study of BSA with the Rh(III) complex, a larger grid map with dimensions of 184 × 184 × 184 Å^3 along the *x, y,* and *z* directions with grid-point spacing of 0.6 Å was generated. Similar to DNA, BD and FD were performed to find the best site for the interaction of the complex with BSA.

The structures of DNA + complex and BSA + complex, obtained from the docking with Hex 6.1 software, were used as initial structures for doing focus docking, considering the ligand flexible, with Autodock 4.2 software.[32] The dimension of the grid map and grid point spacing for DNA and BSA were the same as those used for the docking with Hex software.

ONIOM Calculations

To have a more accurate estimation for the electronic interaction of the Rh(III) complex with DNA and calculation of the electronic interaction energy in two different environments including the gas phase and water, the Our own N-layered Integrated molecular Orbital and molecular Mechanics (ONIOM) method[33] was used. Two different ONIOM schemes, two-layer (QM/QM) and three-layer (QM/QM/MM), were employed for the calculations in the gas phase and water, respectively.

(a) *Gas phase*: For the optimization of the Rh(III) complex + DNA in the gas phase, two-layer ONIOM calculations, the Rh(III) complex and DNA were considered as high- and low-layer, respectively, and quantum mechanical methods were used for both layers (QM/QM).

The geometry of the Rh(III) complex–DNA system obtained from the molecular docking calculations in the previous section was used as the starting geometry for the ONIOM calculations in the gas phase. The density functional theory (DFT) method employing B3LYP functional was used for the high-layer (Rh(III) complex) and the semi-empirical method (PM6)[34] was selected for the low-layer (DNA) of the ONIOM system. The relativistic effective core pseudo-potential LANL2DZ was used as the basis set for all atoms of the Rh(III) complex in the DFT calculations.

(*b*) *water*: For the optimization of the Rh(III) complex + DNA in water, three-layer ONIOM calculations, the Rh(III) complex was selected as high-layer part of the system; DNA and water molecules were considered as medium- and low-layer parts of the system, respectively. The quantum mechanical methods were used for high and medium parts of the system and the molecular mechanic method was used for the low part of the system (QM/QM/MM). Similar to the previous section, the initial geometry of (DNA + complex) obtained from the molecular docking study was employed for the ONIOM calculations in water. For this purpose, the structure of the Rh(III) complex + DNA was embedded in a periodic box ($30 \times 30 \times 45$ Å^3) of pre-equilibrated water molecules (containing 983 molecules) at $T = 300$ K and 1 atm using the Hyperchem 8 software.[35] The pre-equilibration of water molecules in the periodic box is performed using TIP3P force field automatically in the Hyperchem software. The system (DNA + Rh(III) complex + water molecules) was more optimized employing the molecular-mechanics method (MM) under periodic boundary conditions by the universal force field (UFF) [36] using the Gaussian software. Generally, there are three force fields in the Gaussian software including UFF, Amber, and Dreiding. Only the UFF field has the force field of metals. The geometry of the complex was frozen during the optimization while the water molecules and DNA were considered relaxed. The optimized structure obtained from the MM method was used as initial geometry for the three-layer ONIOM optimization. The

system was divided into three-layer including a high-layer (complex), a medium-layer (DNA), and a low-layer (water molecules). The B3LYP/LANL2DZ level of theory and PM6 method were used for the complex and DNA, respectively, and the MM method using the UFF force field was employed for the water molecules (B3LYP/LANL2DZ:PM6:UFF). As known, the phosphate groups of DNA are deprotonated at physiological pH. Therefore, for each phosphate group, one positive ion (Na^+) was added to the system to neutralize the negative charge of the phosphate group in the calculations. All of the ONIOM calculations in this work were performed using the Gaussian 09 quantum chemistry package.[37]

Results and discussion

Synthesis and crystal structure

The mononuclear Rh(III) complex was synthesized in good yield (83%) (Scheme 1), by addition of an alcoholic solution of 4,5-diazafluoren-9-one (Scheme 2) to a chloroform solution of the dinuclear Rh(III) complex in a stoichiometric ratio of 2:1 at reflux temperature. The air stable light brown crystals were grown by ether diffusion into an acetonitrile solution of the complex. The crystal structure was characterized successfully by X-ray diffraction analysis.

(Scheme 1)

(Scheme 2)

For overcoming the greater inertness of Rh(III) toward substitution reaction, refluxing operation was essential. Because of the poor solubility of [Rh(phpy-$\kappa^2N,C^{2'}$)$_2$(dafone)]Cl in common organic solvents, the chloride salt of the complex was dissolved in a minimum amount of water and then excess amount of NH_4PF_6 was added to the solution. The yellow precipitate, [Rh(phpy-$\kappa^2N,C^{2'}$)$_2$(dafone)]PF_6, was formed and readily recrystallized. The perspective view (ORTEP) of the complex is shown in Fig. 1 and its selected bond lengths

and angles are gathered in Table 1. As shown in Fig. 1, the complex exhibits a distorted octahedral geometry with the Rh atom located on an inversion center. The Rh(III) center is chelated to two phpy-$\kappa^2N,C^{2'}$ ligands oriented in a *cis* geometry and to a dafone ligand. The dafone ligand is coordinated to the Rh(III) through its nitrogen atoms. The σ-bonded phenyl groups of pyridine-2-yl-2-phenyl ligands are *trans* to the nitrogen atoms of the dafone ligand.

(Fig. 1)

(Table 1)

Spectroscopic studies of the complex

The ^{1}H NMR spectral data for the cyclometallated Rh(III) complex were measured in DMSO-d_6 using TMS as an internal standard. The ^{1}H NMR spectrum of the complex indicates 11 chemical shifts (see Experimental Section) and a diamagnetic behavior for this complex at room temperature. The IR spectrum of free dafone exhibits a band at 1715 cm^{-1} that is attributed to the stretching frequency of the C=O bond.[38] While the IR spectrum of [Rh(phpy-$\kappa^2N,C^{2'}$)$_2$(dafone)]PF_6 shows this absorption band, ν(C=O), at 1739 cm^{-1}. Since the C=O moiety is far removed from the site of coordination of this ligand with the metal ion, this band was not shifted much in the corresponding complexes.[39] The strong band at 843 cm^{-1} is assigned to ν(P–F) that shows the existence of PF_6^- as a counter ion in this complex.[40] The electronic absorption spectrum of the complex was recorded in acetonitrile solution (Fig. S1, ESI†). The absorption bands observed in the UV region (239, 259, and 296 nm) are attributed to ligand-centered ($\pi \rightarrow \pi^*$) transitions.[39] Since the absorption band at 359 nm is not present in the spectra of the ligands, it must be assigned to metal-to-ligand charge transfer (MLCT) transition ($d\pi \rightarrow \pi^*$) involving either the dafone or the phpy-$\kappa^2N,C^{2'}$ ligand. For the cyclometallated $[Rh(\hat{C}N)_2(N–N)]^+$ complexes, an absorption band seen around 370 nm is constant with respect to the polypyridyl co-ligands (N–N) and this band is attributed to Rh →

ĈN.[41,42] Consequently, the absorption band at 359 nm is probably due to the Rh → phpy transition.

DNA-binding properties

Because DNA is one of the potential target site for transition metal anticancer compounds and DNA-binding is the critical step for the study of effective metal-based drugs, the investigation of binding of rhodium complex to the double helix DNA is very important in understanding the mechanism of tumor inhibition for the treatment of the cancer. Thus, to further demonstrate the mechanism of anticancer action of the Rh(III) complex, its interaction with fish sperm DNA (FS-DNA) was analyzed by spectroscopic techniques. Spectral methods are powerful tools for the study of drug binding with biomolecules, since they allow nonintrusive measurements of substances in low concentration under physiological conditions.[43] In this study, the techniques that have been used to characterize and distinguish the binding mode of the Rh(III) complex to DNA, are UV–Vis, fluorescence, and viscosity measurement.

Electronic absorption titration

In order to investigate the possible binding modes and to calculate the binding constant (K_b), the interaction of the Rh(III) complex with FS-DNA was studied by electronic absorption. On incremental addition of DNA, the decrease of the intensity at λ_{max} = 303 nm was observed (Fig. 2). The observed hypochromic changes without red-shift in the UV spectrum of the complex suggest a groove binding preference of the complex over an intercalative mode of DNA binding.[44] As can be seen in Fig. 1, the Rh(III) complex is not planner due to the angles between the ring planes of the aromatic ligands (Table 1). Therefore, it is expected that the full intercalation of the complex with DNA is relatively difficult and characteristics of the complex such as geometry, size and hydrophobicity of the ligands could be effective on the DNA groove binding of the complex. [15]

In order to further investigate the intensity of the interaction between the complex and FS-DNA, the intrinsic binding constant (K_b) was calculated from the decay of the absorbance at 303 nm with increasing concentration of DNA and using Equation (1):[45]

$$[DNA]/(\varepsilon_a - \varepsilon_f) = [DNA]/(\varepsilon_b - \varepsilon_f) + 1/K_b\,(\varepsilon_b - \varepsilon_f) \quad (1)$$

where, [DNA] is the concentration of DNA in base pairs, ε_a, ε_f, and ε_b are the extinction coefficients of the Rh(III) complex at a given DNA concentration, the free Rh(III) complex in solution, and the Rh(III) complex fully bound to DNA, respectively. In plot of $[DNA]/(\varepsilon_a - \varepsilon_f)$ *vs.* [DNA], the obtained K_b value by a linear fit of the data was 1.50×10^4 M^{-1} for the Rh(III) complex, determined by the ratio of the slope to the intercept (inset in Fig. 2).

(Fig. 2)

Fluorescence quenching and competitive binding

The fluorescence measurement was carried out to further clarify the interaction mode between the complex and DNA. After being studied the interaction of the Rh(III) complex with DNA, it was observed that this complex does not have any fluorescence at room temperature either in solution or in the presence of increasing amounts of FS-DNA. Thus, the binding to DNA cannot be directly predicted through the emission spectrum. The interaction of water molecules with transition metal complex results in quenching of its luminescence emission, but the intercalation of the complex with DNA can reduce this water effect and increase the luminescence intensity. Thus, the binding of the Rh(III) complex to FS-DNA has been studied by a competitive binding fluorescence experiment using ethidium bromide (EthBr) as a probe and the Rh(III) complex as a quencher. EthBr, one of the most sensitive fluorescent probes, does not have any considerable emission in an aqueous solution, but it has an extreme fluorescence in the presence of DNA, due to its strong intercalation between the adjacent DNA base pairs.[46] This fluorescence emission can be quenched by the addition of a metal complex as a result of the replacement of EthBr, and/or electron transfer from the

excited EthBr molecule to it.[47] Upon addition of the Rh(III) complex to the DNA–EthBr system, a slight decrease in the fluorescence intensity of EthBr was observed (inset in Fig. 3), revealing that it is not very efficient in competing with the strong intercalator EthBr for the intercalative binding sites.[44] To determine the extent of binding intensity between the metal complex and DNA that is parallel to the extent of fluorescence quenching intensity of the EthBr molecule bound to DNA, the classical Stern–Volmer equation (Equation (2))[48] was used:

$$I_0/I = 1 + K_{sv}[Q] \quad (2)$$

where, [Q] is the concentration of the Rh(III) complex (quencher), K_{sv} is the Stern–Volmer quenching constant, and I_0 and I are the fluorescence intensities in the absence and presence of the quencher, respectively. The fluorescence quenching curve of the DNA-bound EthBr by the complex shows a good agreement (R^2 = 0.98) with the linear curve of the Stern–Volmer equation (Fig. 3) and K_{sv} = 8.6 × 10^4 M^{-1} for this complex is determined by plotting I_0/I *vs.* the complex concentration. The value of K_{sv} expresses that the Rh(III) complex shows a reasonable quenching efficiency and a moderately degree of binding to FS-DNA.

(Fig. 3)

Viscosity measurement

Viscosity measurements, which are sensitive to the length changes of DNA, provide useful information about the metal complex binding mode to DNA in solution. Thus, in order to gain further insight about the nature of interaction between the Rh(III) complex and FS-DNA, the viscosity measurement was carried out. The relation between the relative viscosity (η/η_0) and DNA length (L/L_0) is $L/L_0 = (\eta/\eta_0)^{1/3}$, where, η and L are the respective specific viscosity and the molecular length of DNA at a given complex/DNA ratio, and η_0 and L_0 are the corresponding values for DNA alone.[49] A classical intercalator such as EthBr, due to its insertion between the DNA base pairs and consequently to the lengthening of the DNA

double helix, shows a significant increase in the DNA viscosity.[50] In contrast, groove binding molecules cause little or no effect on the relative viscosity of DNA solution.[51,52] The effect of the complex on the viscosity of FS-DNA has been shown in Fig. S2 (ESI†). Upon addition of the Rh(III) complex, the viscosity of FS-DNA slowly increased but had no very obvious effect on the relative viscosity of FS-DNA. Such behavior further suggests that the Rh(III) complex may probably bind to DNA *via* groove binding mode along with a partial intercalative mode.[51] Thus, the result obtained from the viscosity measurement confirms the mode of the DNA binding of the complex established through absorption and emission spectral studies.

BSA-binding properties

Proteins are considered major targets for therapeutically active complexes. Since that drug–protein interactions immensely influence the absorption, metabolism and distribution of the drugs,[53,54] the investigation of drug–protein interaction is an active field of interest because of the understanding of drug action mechanism and the possibility of designing new and useful medicines. Therefore, the binding properties of the Rh(III) complex with BSA were investigated by UV–Vis and fluorescence techniques.

Absorption spectral studies

UV–Vis absorption spectrum can be used to understand the structural changes of the protein and the protein–drug complex formation. As shown in Fig. 4, the absorption spectra of BSA in the absence and presence of the Rh(III) complex have been recorded at room temperature. BSA has two main absorption bands: one strong absorption peak in the range of 208–240 nm, which is ascribed to the $\pi \rightarrow \pi^*$ transition of the polypeptide backbone structure C=O of BSA[15] and also, represents the content of α-helix in the protein[55] and one weak absorption peak at about 278 nm due to the $\pi \rightarrow \pi^*$ transition of the aromatic amino acids (Trp, Tyr, and Phe).[15]

(Fig. 4)

Fig. 4 depicts that the intensity of the BSA absorption peak in 218 nm obviously decreased and shifted toward longer wavelength as the complex was added. This dramatic decrease can be attributed to the induced perturbation of the α-helix of protein by a specific interaction with the ligands.[55,56] Furthermore, the obvious red shift on the absorption spectrum is due to the effect of the polar solvent (water) and perturbations in the microenvironment of the polypeptide backbone of the protein in the presence of the Rh(III) complex. Water stabilizes the energy of the π^* electron cloud more than the π electron cloud (water lowers the energy levels of both the states). Under such a circumstance, the $\pi \rightarrow \pi^*$ transition undergoes a bathochromic shift, because the energy gap between the π–π^* states is decreased.[57] Upon addition an equal amount of the Rh(III) complex to both the BSA solution and the reference solution to eliminate the absorbance of the complex itself, the intensity of the absorbance peak around 278 nm enhanced and there was a little blue shift. These observations indicate that the hydrophobicity increased,[58] and more aromatic acid residues were extended into the aqueous environment.[59] Overall, the changes in the absorbance spectra show that the Rh(III) complex interacts with the BSA molecule and the microenvironment of the three aromatic acid residues is altered and also, the interaction between the Rh(III) complex and BSA is mainly a static quenching process.[56]

Fluorescence spectroscopic studies

The fluorescence spectroscopy can be utilized to determine the molecular interaction of the Rh(III) complex with BSA. BSA has strong fluorescence emission. The fluorescence emission spectra of BSA were recorded in the absence and presence of different concentrations of the Rh(III) complex (inset in Fig. 5). As shown in this Figure, BSA has a strong fluorescence emission peak at 347 nm. The fluorescence intensity of BSA decreased regularly with increasing concentration of the Rh(III) complex, while the emission maximum

wavelengths and shape of the peaks remained almost unchanged. This showed that the Rh(III) complex could bind to BSA and quench its intrinsic fluorescence. The 'inner-filter effect' commonly arises if there is any absorption of the molecule added during fluorescence titration at the wavelength of excitation or at the wavelength used to note the emission, and the results of which is spurious decrease in the observed fluorescence intensity.[60] In order to correct the inner-filter effect, the following equation (Equation (3))[61] was used:

$$I_{corr} = I_{obs} \exp(½A_{ex} + ½A_{em}) \quad (3)$$

Where, I_{corr} is the corrected fluorescence in the absence of inner-filter effect, I_{obs} is the measured fluorescence, and A_{ex} and A_{em} are the absorption values at excitation and emission wavelength, respectively. The quenching of the BSA fluorescence may take place by dynamic (resulting from collisional encounters between the fluorophore and the quencher) or static (resulting from the formation of a ground-state complex between the fluorophore and the quencher) mechanism.[62] In order to study the quenching mechanism between the complex and BSA, the fluorescence quenching data were analyzed using the Stern–Volmer equation (Equation (4)):[63]

$$I_0/I = 1 + K_{sv}[Q] = 1 + k_q\tau_0[Q] \quad (4)$$

where, $[Q]$ is the concentration of the drug (quencher), I_0 and I are the fluorescence intensities at the maximum wavelength in the absence and presence of the drug after correction for the inner-filter effect, respectively, and K_{sv} is the Stern–Volmer quenching constant which was determined by linear regression of a plot of I_0/I *vs.* $[Q]$ (Fig. 5). k_q is the quenching rate constant of biomolecule and τ_0 is the average lifetime of the fluorophore without the quencher with the value of 10^{-8} s for the biopolymer.[64]

(Fig. 5)

The quenching rate constant calculated in this equation is $k_q = K_{sv}/\tau_0$. In dynamic quenching, the value of k_q is limited to 2.0×10^{10} M^{-1} s^{-1}.[65] The k_q value for the Rh(III)

complex is 1.36×10^{14} M^{-1} s^{-1}. Here, the obtained value is greater from that of value suggested in dynamic quenching. So, this result confirms that a non-fluorescent complex was formed between the fluorophore and the drug, *i.e.* a static quenching mechanism. Thus, the Rh(III) complex was located at close proximity to the tryptophan residue for quenching to occur.

Binding constant and the number of binding sites

For the static quenching interaction, if it is assumed that there are similar and independent binding sites in the biomolecule, the binding constant (K_b) and the number of binding sites per albumin or DNA molecule (n) can be determined by the intercept and the slope of the double logarithm regression curve of log $[(I_0 - I)/I]$ *vs.* log $[Q]$ based on the Scatchard equation (Equation (5)):[66]

$$\log (I_0 - I/I) = \log K_b + n \log [Q] \quad (5)$$

where, I_0, I, and $[Q]$ are the same as in Equation (4), K_b is the apparent association constant or the binding constant of the Rh(III) complex to BSA or DNA, and n is the number of the binding sites per albumin or DNA molecule. The correlation coefficients larger than 0.9 show that the assumptions underlying the deviation of Equation (5) are reasonable. The number of the binding sites for the Rh(III) complex on DNA (Fig. S3, ESI†) and BSA (Fig. S4, ESI†) are 0.94 and 1.15, respectively. The values of n for the Rh(III) complex emerged to be ~ 1, that strongly suggests existence of a single binding site in DNA and BSA or in other words, indicates that the $[Rh(phpy\text{-}\kappa^2N,C^{2'})_2(dafone)]^+$ cation forms a complex with a molar ratio 1:1 with DNA and BSA.[15]

The binding constant values determined by the fluorescence quenching experiments show a good conformity with the values of the binding constants obtained from the UV–Vis titrations for the interactions of the Rh(III) complex with DNA and BSA. The binding constant of the Rh(III) complex with BSA (6.0×10^6 M^{-1}) is more than DNA which indicates more binding

affinity of the complex to BSA than DNA. The K_b value is very useful for understanding of the distribution, metabolism, and delivery of drugs. A small binding constant can increase the concentration of free drug in the plasma, while a large binding constant can decrease the concentration of free drug in the plasma and therefore causes a better distribution and the more improved pharmacology effects.[67]

Energy transfer between BSA and the Rh(III) complex

The studies on fluorescence spectroscopy proved that the BSA molecule could form a complex with the Rh(III) complex. To get much more information about the Rh(III) complex–BSA system, our studies were focused on the aspect of energy transfer in this system. According to the Förster's non-radioactive energy transfer theory (FRET), the energy transfer from a protein residue (donor) to a drug (acceptor) occurs under three different conditions: (i) the donor can produce fluorescence light; (ii) fluorescence emission spectrum of the donor and absorbance spectrum of the acceptor have an adequate overlap; and (iii) the distance between the donor and the acceptor species is less than approximately 8 nm.[68] Although there are three types of fundamental fluorophores in BSA, *viz.* tryptophan (Trp), tyrosine (Tyr), and phenylalanine (Phe), but the intrinsic fluorescence of BSA is generally due to tryptophan.[65] The overlap of the absorption spectrum of the Rh(III) complex with the fluorescence emission spectrum of BSA in the wavelength range of 307–507 nm is shown in Fig. S5 (ESI†). According to the Förster's theory, the energy transfer efficiency (E) is related not only to the donor–acceptor distance (r), but also to the critical energy transfer distance (R_0). Thus, the value of E is calculated using Equation (6):[69]

$$E = 1 - \frac{I}{I_0} = \frac{R_0^6}{R_0^6 + r^6} \quad (6)$$

where, I_0 and I are the fluorescence intensities of BSA measured in the absence and presence of the drug, r represents to the acceptor–donor distance, and R_0 is the critical distance when the transfer efficiency is 50%. The value for R_0 can be calculated by Equation (7):[70]

$$R_0^6 = 8.79 \times 10^{-25} K^2 N^{-4} \Phi J \quad (7)$$

where, K^2 is the spatial orientation factor and describes the relative position of the donor and acceptor dipoles, ranging from 0 (perpendicular dipoles) to 4 (parallel dipoles). Generally, the dipoles are supposed to be rapidly moving, on timescales similar to the donor excited-state lifetime, and their orientations are therefore described randomly with K^2 = 2/3, N is the average refractive index of the medium in the wavelength range where spectral overlap is significant (= 1.336), Φ is the fluorescence quantum yield of the donor in the absence of the acceptor (= 0.15), and J is the overlap integral between the emission spectrum of the donor and the absorption spectrum of the acceptor. The J value is given by Equation (8):[71]

$$J = \frac{\sum F(\lambda)\varepsilon(\lambda)\lambda^4 \Delta\lambda}{\sum F(\lambda)\Delta\lambda} \quad (8)$$

where, $F(\lambda)$ is the fluorescence intensity of the fluorescent donor at wavelength λ and $\varepsilon(\lambda)$ is the molar absorption coefficient of the acceptor at wavelength λ. The Rh(III) complex absorbs where BSA fluoresces (347 nm). Therefore, the data were corrected using Equation 3.[60] The J value was calculated to be 8.426×10^{-20} cm^3 L mol^{-1}, and the values for R_0, r , and E were calculated to be 3.64 nm, 4.33 nm, and 0.26, respectively. The obtained value for the distance from the Rh(III) complex to the tryptophan residue of the protein, $r < 8$ nm, that is in conform with essential conditions for FRET, indicating that the energy transfer from BSA to the Rh(III) complex occurs with high possibility.[72] Furthermore, It was suggested that the binding of the complex to BSA was formed through energy transfer, which quenched the fluorescence of BSA molecules, indicating the presence of static quenching interaction between BSA and the Rh(III) complex.[73] Also, the greater r value compared with that of R_0 confirms the static quenching mechanism.[74]

Biological activity studies

The results obtained from DNA/protein binding and molecular docking studies prompted us to explore anticancer activity of the Rh(III) complex. The influence of this complex on the proliferation of HepG2, HT-29, and SH-SY5Y tumor cell lines was examined by the 3-(4,5-dimethylthiazol-2-yl)-2,5-diphenyltetrazolium bromide (MTT) assay.[75] Fig. 6 shows plot of the percentage inhibition *vs.* the concentration of the Rh(III) complex (0.5–40 μM). The results show that the cell viability of the cancer cells was strongly decreased with increasing the concentration of the complex and had a concentration-dependent manner. The cytotoxic activity of this complex was measured through the spectrophotometric data by means of Equation (9):[76]

$$\% \text{ cell cytotoxicity} = [1 - \text{Abs(drug)}/\text{Abs(control)}] \times 100 \quad (9)$$

where, Abs(drug) and Abs(control) are the average absorbance of the treated cells with the compound and non-treated cells served as controls, respectively. The IC_{50} values of the compound and the IC_{50} values obtained for the *cis*platin complex, to compare the cytotoxic activity with the synthesized complex under analogous conditions, have been shown in Table 2. These results indicate that the Rh(III) complex is active and exhibits significant cytotoxic effects against the selected tumor cell lines.

(Fig. 6)

(Table 2)

Molecular docking of the Rh(III) complex with DNA

Molecular docking techniques are well-documented computational tools to understand the Drug–DNA interactions for structure-based drug design and discovery, as well as mechanistic study by placing a small molecule into the binding site of the target specific region of DNA mainly in a non-covalent fashion. In this study, the focus docking (FD) was performed on the best location obtained by the blind docking (BD), a binding site with the best free energy

binding (ΔG_b), –7.5 kcal mol^{-1}, was found for the interaction of the Rh(III) complex with DNA, indicating a high binding affinity between DNA and the complex. The corresponding value obtained from the experimental value of K_b (1.5×10^4 M^{-1}) is about –5.73 kcal mol^{-1} (Table 3) that shows the obtained result by absorption titration was comparable to the value calculated through the computational method. Fig. 7 (*a*) demonstrates the molecular docking and the binding site of the complex interacting with DNA and Fig. 7 (*b*) shows the bases of DNA which have dominant interactions with the complex in the interaction region. The interaction scheme of the residues of binding site of DNA with the Rh(III) complex generated by the LIGPLOT+ software has been shown in Fig. 8. It can be seen that the dominant interactions between the complex and the residues in the active site are hydrophobic interactions (Type and number of interactions, ESI†).

(Fig. 7)

(Fig. 8)

Molecular docking of the Rh(III) complex with BSA

The binding mode and intermolecular interaction of the Rh(III) complex with BSA were investigated by molecular docking to suggest the most acceptable mechanism for this interaction. The best value of ΔG_b for the interaction of the complex with BSA was found to be –8.3 kcal mol^{-1} that indicates a good binding affinity between the Rh(III) complex and BSA. It was comparable to its corresponding value (–9.30 kcal mol^{-1}) obtained from the experimental value of K_b (6.0×10^6 M^{-1}) of the complex and BSA (Table 3). Fig. 9 (*a*) shows the complex docked into the binding site of the BSA protein generated by the PyMol software.[77] Also, the residues of the protein interacting with the complex in the binding site are magnified in Fig. 9 (*b*). Fig. 10 shows the two-dimensional scheme of the interaction between the complex and BSA generated by the LIGPLOT+ software. There are hydrophobic interactions between the complex and BSA (Type and number of interactions, ESI†).

(Table 3)

(Fig. 9)

(Fig. 10)

The values of r (donor–acceptor distance) and R_0 (critical energy transfer distance) obtained from the Förster's theory are about 4.33 and 3.64 nm, respectively, that are comparable to the distances between tryptophan and the Rh(III) complex obtained from the docking simulation, where the calculated distances of the complex are 2.85 and 5.02 nm from Trp-134 and Trp-213, respectively.

ONIOM calculations

The Rh(III) complex–DNA system in the gas phase

Fig. 11 demonstrates the optimized structure of (DNA + Rh(III) complex) in the gas phase calculated using the (B3LYP/LANL2DZ:PM6) ONIOM method.

(Fig. 11)

Table 1 compares some structural parameters of the complex–DNA system including bond lengths, bond angles, and dihedral angles in the gas phase with those obtained from the X-ray data. In addition, the structural parameters of the free complex optimized in the gas phase have been also added to this table. For optimizing the free complex in the gas phase, the B3LYP/LANL2DZ level of theory was used.

The Rh(III) complex–DNA system in water

The optimized structure of the Rh(III) complex–DNA in water has been shown in Fig. 12.

(Fig. 12)

Table 1 compares some of the bond lengths, bond angles, and dihedral angles of the complex interacting with DNA in water with those obtained from the X-ray data and the gas phase. Furthermore, the structural parameters of the free complex optimized in the gas phase and water solvent have been added to this table. The B3LYP/LANL2DZ level of theory was

used for optimizing the free complex in both gas and water phases. Also, for modeling the electrostatic effect of water on the free complex, the polarized continuum model (PCM) was used.

It is evident from Fig. 11 that there is a considerable change in the geometry of the complex because of its interaction with DNA in the gas phase, compared to the solid-state structure obtained from crystallography data (Fig. 1). It can be seen that the deformation of the complex structure in the water medium (Fig. 12) is considerably lower than that in the gas phase, because of the complex interaction with the water molecules which prevents from the deformation of its structure by the interaction with DNA compared to the gas phase.

Electronic interaction energy of the Rh(III) complex with DNA in the gas phase and water

The final optimized structures calculated in the previous section for the gas phase and water were used for the ONIOM single-point energy calculations. For calculating the interaction energies in the gas phase and water, the (QM/QM/MM) ONIOM schemes were used. The DFT method employing M062X functional[78] was used for the quantum part of the system (complex and DNA) in both environments. The relativistic effective core pseudo-potential LANL2DZ was used for Rh atom of the complex and the 6-31G(d) basis set was used for the C, H, N and O atoms of the complex. The LANL2DZ was also used for a part of DNA (hexamer-DNA) which includes bases with dominant interactions with the complex. The other part of DNA was considered as an MM part in both calculations in the gas phase and water. The water molecules were also considered as an MM part of the system for the ONIOM calculations in water. The UFF force field was used for the MM region of the calculations in both gas phase and water. The electrostatic and van der Waals (vdW) interactions between the water molecules and the complex + DNA were considered by the QEq formalism implemented in the Gaussian 09 software[37]. As shown in Fig. 13, pictorially,

the interaction energy between the complex and DNA is calculated by two different equations in the gas phase and water.

(Fig. 13)

Fig. 13 (*b*) shows that for obtaining the interaction energy using three-layer ONIOM calculation, two additional single-point two-layer ONIOM calculations on the (DNA + water) and (complex + water) systems, and one MM calculation on the water system are necessary. It should be emphasized that the systems of (DNA + water) and (complex + water) are constructed from the final optimized structure of the system of (the Rh(III) complex + DNA + water) (see Fig. 12) by removing the structure of the complex and DNA, respectively, without any changes in the coordinates of the remaining atoms. The calculated interaction energies between the complex and DNA in the gas phase and water are –814.4199 and –744.444 kcal.mol^{-1}, respectively. It is seen that the presence of the water molecules decreases the interaction of the complex with DNA compared to the gas phase. The reason of the decrease in the interaction energy can be attributed to the lower deformation of the Rh(III) complex structure in water and the effect of the electrostatic field of the water molecules which polarizes the wave function of the complex so that creates repulsive interaction between DNA and the Rh(III) complex. Gkionis et al.[79] performed the QM/MM calculations with two-level ONIOM method (BH and H:Amber96) to calculate the interaction energy between DNA and some platinum-based anticancer drugs. For example, they found that the interaction energies of heptaplatin with octamer-DNA are –638.3 and –337.1 kcal.mol^{-1}, respectively. It is interesting to notice that the calculated interaction energies of the Rh(III) complex in this work are comparable with the interaction energies of the platinum-based complex reported by Gkionis et al.[79] It is notable that the reported interaction energies obtained from the ONIOM calculations are the electronic interaction energies and are not the free binding energy, because the free binding energy is the Gibbs free energy and there is the

contribution of the entropy in it. Therefore, the huge difference between the free binding energy obtained from the docking and the electronic interaction energies obtained from the ONIOM calculations is normal.

The effect of DNA interaction on the UV spectrum of the Rh(III) complex

The interaction of the Rh(III) complex with DNA was interpreted using the calculated UV spectra of the complex. The absorption spectrum of the Rh(III) complex was studied in different environments including free complex in acetonitrile, free complex in water, and complex interacting with DNA in water. The time-dependent density functional theory (TD-DFT) employing M062X functional was used for the calculations of the absorption spectrum of the complex in this part. The LANL2DZ for Rh atom and 6-31+G(d) basis set for the other atoms of the complex were used for the quantum mechanical part of the system. In the TD-DFT calculations, for (DNA + the Rh(III) complex) in the gas phase, the ONIOM (M062X/6-31 + G(d)/LANL2DZ:PM6), and for (DNA + the Rh(III) complex + water), the ONIOM (M062X/6-31 + G(d)/LANL2DZ:PM6:UFF) were used. It is important to notice that the PM6 method was selected for DNA in the calculations of this part. Fifty excited electronic states of the complex were calculated for the TD-DFT calculations. For calculating the absorption spectrum of the free complex in acetonitrile and water, the PCM model was used for modeling the electrostatic field of the solvent. Fig. 14 demonstrates the calculated absorption spectrum of the complex in acetonitrile and compares it with the corresponding experimental spectrum. It can be seen that there is a very good agreement between the theoretical and the experimental spectra which confirms the validity of the synthesized complex in this work. The theoretical spectrum has been shifted to the higher wavelength about 18.5 nm for matching with the experimental spectrum which is in the range of the error of the TD-DFT method in the simulation of the absorption spectra. The vertical narrow lines show the calculated positions and intensities of the absorption bands used for simulating the absorption

spectrum. Four calculated absorption bands (related to the visible absorptions in the experimental spectrum) have been identified with the roman numbers in Fig. 14 (**I**, **II**, **III**, and **IV**).

(Fig. 14)

The absorption line **No. I** located at 338.59 nm is the sixth absorption band of the complex and is related to the excitation of the electron from HOMO to LUMO + 2 (HOMO → LUMO + 2). The intensity of the first to fifth calculated absorption bands of the complex is zero. The absorption line **No. II** corresponds to the twelfth absorption band of the complex and the wave function of the excited state accessible through this excitation is a linear combination of three excited Kohn-Sham determinants related to the HOMO – 2 → LUMO (39%), HOMO – 1 → LUMO + 3 (30%), and HOMO → LUMO + 2 (31%) excitations. The numbers in parentheses are the contributions of the excitation in the absorption line. The absorption line **No. III** is related to the excitation of the complex from the ground state to the twenty sixth excited state. The wave function of the excited state of this transition is a linear combination of two excited Kohn-Sham determinants related to the HOMO – 1 → LUMO + 3 (49%) and HOMO → LUMO + 5 (51%) excitations. The last absorption line (**No. IV**) is the forty third absorption band of the complex related to the HOMO – 6 → LUMO + 2 (32%), HOMO – 7 → LUMO + 3 (26%), and HOMO – 15 → LUMO (41%) excitations. The shapes of the molecular orbitals involved in the transitions related to the absorption lines **I**, **II**, **III**, and **IV** have been demonstrated in Fig. 15. The HOMO of the complex is mainly related to the *d* orbital of the Rh atom while the LUMO has π character and is a π^* orbital of the ligand. Similarly, as seen in Fig. 15, both HOMO – 7 and HOMO – 6 are mainly localized on the ligand part of the complex. The other molecular orbitals presented in this Figure have contribution from the ligand and the *d* orbitals of the central metal.

(Fig. 15)

To confirm the effect of interaction of the complex with DNA on the absorption spectrum of the complex shown in Fig. 2, the absorption spectrum of the free complex in water and the complex interacting with DNA were calculated in this part, separately. Fig. 16 demonstrates the calculated spectra of the complex with and without interaction with DNA and compares them with the corresponding experimental spectra. It can be seen that the interaction of the complex with DNA reduced the intensity of the experimental spectrum for $\lambda < 330$ nm and the feature assigned with green asterisk disappeared. It can be seen that the theoretical calculations interestingly confirm the reduction in the intensity of the spectrum due to the interaction of the complex with DNA in water. Similar to the experimental spectra, the peak assigned with the red asterisk in the calculated spectrum of the free complex in water is omitted in the calculated spectrum of the complex interacting with DNA in water.

(Fig. 16)

Conclusion

A new cyclometallated Rh(III) complex, $[Rh(phpy\text{-}\kappa^2N,C^{2'})_2(dafone)]PF_6$, was prepared and structurally characterized by spectroscopic methods and X-ray crystallography. The results show that the complex has a distorted octahedral geometry. The biological properties of the complex were studied by the experimental and theoretical methods. The interaction of the complex with FS-DNA was monitored by viscosity measurement, spectroscopic and molecular docking methods. The results indicate that the Rh(III) complex can bind to DNA *via* groove binding mode along with a partial intercalative interaction. Also, the binding propensity of the complex to BSA was investigated by absorption and fluorescence techniques in combination with molecular modeling. The results suggest that the hydrophobic bonding interactions play major role in the binding of the Rh(III) complex to BSA. Furthermore, the *in vitro* anticancer activity of the complex against the HepG2, HT-29, and

SH-SY5Y cells using the MTT assay suggests that the Rh(III) complex is a potential anticancer candidate. The QM/QM and QM/QM/MM methods in the gas phase and water, respectively, were used to interpret the interaction of the Rh(III) complex with DNA by the ONIOM calculations. The effect of the interaction of the Rh(III) complex with DNA on the experimental and theoretical absorption spectra shows that both experimental and theoretical investigations confirm each other.

Electronic Supplementary Information (ESI)

Table S1; Type and number of interactions (Table S2); Figures illustrating: electronic spectrum of the Rh(III) complex (Fig. S1), Relative viscosity of DNA in the presence of the Rh(III) complex (Fig. S2), the Rh(III) complex–DNA binding constant and the number of the binding sites on DNA (Fig. S3), the Rh(III) complex–BSA binding constant and the number of the binding sites on BSA (Fig. S4), Spectral overlap of the absorption of the Rh(III) complex with the BSA fluorescence spectrum (Fig. S5). CCDC 1057307 contains the supplementary crystallographic data for this paper. These data can be acquired free of charge from The Director, CCDC, 12 Union Road, Cambridge CB2 1EZ, UK (fax: +44-1223-336033; e-mail: deposit@ccdc.cam.ac.uk or http://www.ccdc.cam.ac.uk).

Acknowledgement

We are grateful to the Isfahan University of Technology (IUT) for financial support.

References

1 U. Śliwińska, F. P. Pruchnik, I. Pelińska, S. Ułaszewski, A. Wilczok and A. Zajdel, *J. Inorg. Biochem.*, 2008, **102**, 1947.

2 M. Ćwikowska, F. P. Pruchnik, R. Starosta, H. Chojnacki, A. Wilczok and S. Ułaszewski, *Inorg. Chim. Acta*, 2010, **363**, 2401.

3 R. F. M. Frade, N. R. Candeias, C. M. M. Duarte, V. André, M. T. Duarte, P. M. P. Gois and C. A. M. Afonso, *Bioorg. Med. Chem. Lett.*, 2010, **20**, 3413.

4 D. E. Morrison, J. B. Aitken, M. D. de Jonge, F. Issa, H. H. Harris and L. M. Rendina, *Chem. Eur. J*., 2014, **20**, 16602.

5 H. Huang, P. Zhang, H. Chen, L. Ji and H. Chao, *Chem. Eur. J*., 2015, **21**, 715.

6 D. Sardar, P. Datta, S. Das, B. Saha, S. Samanta, D. Bhattacharya, P. Karmakar, C. Chen, C. Chen and C. Sinha, *Inorg. Chim. Acta*, 2013, **394**, 98.

7 T. Mukherjee, B. Sen, A. Patra, S. Banerjee, G. Hundal and P. Chattopadhyay, *Polyhedron*, 2014, **69**, 127.

8 A. Dorcier, C. G. Hartinger, R. Scopelliti, R. H. Fish, B. K. Keppler and P. J. Dyson, *J. Inorg. Biochem.*, 2008, **102**, 1066.

9 S. Top, I. Efremenko, M. N. Rager, A. Vessiéres, P. Yaswen, G. Jaouen and R. H. Fish, *Inorg. Chem.*, 2011, **50**, 271.

10 J. L. Kisko and J. K. Barton, *Inorg. Chem.*, 2000, **39**, 4942.

11 W. L. Su, Y. C. Yu, M. C. Tseng, S. P. Wang and W. L. Huang, *Dalton Trans.*, 2007, 3440.

12 M. Lau, K. Cheung, Q. Zhang, Y. Song, W. Wong, I. D. Williams and W. Leung, *J. Organomet. Chem*., 2004, **689**, 2401.

13 K. Sünkel, M. Graf, H. Böttcher, B. Salert and H. Krüger, *Inorg. Chem. Commun*., 2011, **14**, 539.

14 (a) R. H. Fish, *Coord. Chem. Rev.*, 1999, **185–186**, 569. (b) D. P. Smith, H. Chen, S. Ogo, A. I. Elduque, M. Eisenstein, M. M. Olmstead and R. H. Fish, *Organometallics*, 2014, **33**, 2389.

15 F. Hajareh Haghighi, H. Hadadzadeh, F. Darabi, Z. Jannesari, M. Ebrahimi, T. Khayamian, M. Salimi and H. Amiri Rudbari, *Polyhedron*, 2013, **65**, 16.

16 U. Śliwińska-Hill, F. P. Pruchnik, M. Latocha, D. Nawrocka-Musiał and S. Ułaszewski, *Inorg. Chim. Acta*, 2013, **400**, 26.

17 J. D. Aguirre, D. A. Lutterman, A. M. Angeles-Boza, K. R. Dunbar and C. Turro, *Inorg. Chem*., 2007, **46**, 7494.

18 J. D. Aguirre, A. M. Angeles-Boza, A. Chouai, C. Turro, J. Pellois and K. R. Dunbar, *Dalton Trans.*, 2009, 10806.

19 S. Mukhopadhyay, R. K. Gupta, R. P. Paitandi, N. K. Rana, G. Sharma, B. Koch, L. K. Rana, M. S. Hundal and D. S. Pandey, *Organometallics*, 2015, **34**, 4491.

20 J. H. van Diemen, J. G. Haasnoot, R. Hage, J. Reedijk, J. G. Vos and R. Wang, *Inorg. Chem*., 1991, **30**, 4038.

21 SAINT, Version 6.02, Bruker Analytical X-ray System, Inc., Madison, Wisconsin, USA, 1999.

22 M. C. Burla, R. Caliandro, M. Camalli, B. Carrozzini, G. L. Cascarano, L. De Caro, C. Giacovazzo, G. Polidori and R. Spagna, *J. Appl. Crystallogr.*, 2005, **38**, 381.

23 (a) G. M. Sheldrick, SHELXL97, Program for Crystal Structure Refinement, University of Göttingen, Göttingen, Germany, 1997. (b) L. N. Shelxt, Version 5.10, Bruker Analytical X-ray System, Inc., Madison, WI, USA, 1998.

24 J. Marmur, *J. Mol. Biol*., 1961, **3**, 208.

25 G. Cohen and H. Eisenberg, *Biopolymers*, 1969, **8**, 45.

26 A. Hussain, S. Gadadhar, T. K. Goswami, A. A. Karande and A. R. Chakravarty, *Eur. J. Med. Chem*., 2012, **50**, 319.

27 http://www.loria.fr/~ritchied/hex/

28 http://www.rcsb.org.

29 D. W. Ritchie and G. J. L. Kemp, *J. Comput. Chem*., 1999, **20**, 383.

30 D. van der Spoel and C. Hetényi, *Protein Sci.*, 2002, **11**, 1729.

31 C. Hetényi and D. van der Spoel, *FEBS Lett*., 2006, **580**, 1447.

32 G. M. Morris, R. Huey, W. Lindstrom, M. F. Sanner, R. K. Belew, D. S. Goodsell and A. J. Olson, *J. Comput. Chem.*, 2009**, 16**, 2785. Autodock4 and AutoDockTools4: automated docking with selective receptor flexibility.

33 S. Dapprich, I. Komáromi, K. S. Byun, K. Morokuma and M. J. Frisch, *J. Mol. Struct.*, 1999, **462**, 1.

34 J. P. Stewart, *J. Mol. Model*., 2007, **13,** 1173.

35 HyperChem, *HyperChem Release 8.0 for Windows*, Hypercube, Inc., Florida, USA.

36 A. K. Rappé, C. J. Casewit, K. S. Colwell, W. A. G. III and W. M. Skiff, *J. Am. Chem. Soc*., 1992, **114**, 10024.

37 M. J. Frisch, G. W. Trucks, H. B. Schlegel, G. E. Scuseria, M. A. Robb, J. R. Cheeseman, G. Scalmani, V. Barone, B. Mennucci, G. A. Petersson and et al. *Gaussian 09*, revision B.01; Gaussian, Inc., Wallingford, CT, 2009.

38 A. R. Biju and M. V. Rajasekharan, *Polyhedron*, 2008, **27**, 2065.

39 G. Mansouri, A. R. Rezvani, H. Hadadzadeh, H. R. Khavasi and H. Saravani, *J. Organomet. Chem.*, 2007, **692**, 3810.

40 K. Nakamato, Infrared and Raman Spectra of Inorganic and Coordination Compounds Part II: Application in Coordination, Organometallic and Bioinorganic Chemistry, 5th ed. Wiley-Inter-science, New York, 1997.

41 H. Hadadzadeh, A. R. Rezvani and F. Belanger-Gariepy, *J. Mol. Struct*., 2005, **740**, 165.

42 M. G. Colombo, T. C. Brunold, T. Riedener, H. U. Güdel, M. Fortsch and H. B. Bürgi, *Inorg. Chem*., 1994, **33**, 545.

43 E. Liu, L. Qi and P. Li, *Molecules*, 2010, **15**, 9092.

44 R. Loganathan, S. Ramakrishnan, M. Ganeshpandian, N. Bhuvanesh, M. Palaniandavar, A. Riyasdeen and M. A. Akbarsha, *Dalton Trans.*, 2015, **44**, 10210.

45 A. Wolfe, G. H. Shimer and T. Meehan, *Biochemistry*, 1987, **26**, 6392.

46 I. Haq, P. Lincoln, B. Norden, B. Z. Chowdhry and J. B. Chaires, *J. Am. Chem. Soc*., 1995, **117**, 4788.

47 S. Mathur and S. Tabassum, *BioMetals,* 2008, **21**, 299.

48 J. R. Lakowicz and G. Weber, *Biochemistry*, 1973, **12**, 4161.

49 Y. Geldmacher, R. Rubbiani, P. Wefelmeier, A. Prokop, I. Ott and W. S. Sheldrick, *J. Organomet. Chem*., 2011, **696**, 1023.

50 S. Anbu, S. Kamalraj, B. Varghese, J. Muthumary and M. Kandaswamy, *Inorg. Chem*., 2012, **51**, 5580.

51 B. Maity, M. Roy, S. Saha and A. R. Chakravarty, *Organometallics,* 2009**, 28***,* 1495.

52 B. Maity, M. Roy, B. Banik, R. Majumdar, R. R. Dighe and A. R. Chakravarty, *Organometallics*, 2010, **29**, 3632.

53 A. Das, R. Chitra, R. R. Choudhury and M. Ramanadham, *Pramana*, 2004, **63**, 363.

54 N. Wang, L. Ye, B. Q. Zhao and J. X. Yu, *Braz. J. Med. Biol. Res*., 2008, **41**, 589.

55 J. Ruiz, C. Vicente, C. de Haro and D. Bautista, *Inorg. Chem*., 2013, **52**, 974.

56 F. Samari, B. Hemmateenejad, M. Shamsipur, M. Rashidi and H. Samouei, *Inorg. Chem*., 2012, **51**, 3454.

57 B. K. Paul, K. Bhattacharjee, S. Bose and N. Guchhait, *Phys. Chem. Chem. Phys*., 2012, **14**, 15482.

58 J. Abraham and B. Mathew, *Res. J. Recent Sci*., 2014, **3**, 157.

59 A. Mallick, S. Chandra, S. Maiti and N. Chattopadhyay, *Biophys. Chem*., 2004, **112**, 9.

60 J. R. Lakowicz, "*Principles of Fluorescence Spectroscopy"*, Springer, US, 3rd edn, 2006.

61 M. Van de Weert and L. Stella, *J. Fluoresc*., 2010, **20**, 625.

62 R. P. Paitandi, R. K. Gupta, R. S. Singh, G. Sharma, B. Koch and D. S. Pandey, *Eur. J. Med. Chem.*, 2014, **84**, 17.

63 M. R. Eftink and C. A. Ghiron, *Anal. Biochem*., 1981, **114**, 199.

64 J. R. Lakowicz and G. Weber, *Biochemistry*, 1973, **12**, 4171.

65 Z. Jannesari, H. Hadadzadeh, T. Khayamian, B. Maleki and H. Amiri Rudbariand, *Eur. J. Med. Chem*., 2013, **69**, 577.

66 M. Jiang, M. X. Xie, D. Zheng, Y. Liu, X. Y. Li and X. Chen, *J. Mol. Struct*., 2004, **692**, 71.

67 P. Bourassa, S. Dubeau, G. M. Maharvi, A. H. Fauq, T. J. Thomas and H. A. Tajmir-Riahi, *Eur. J. Med. Chem*., 2011, **46**, 4344.

68 Y. Zhang, S. Shi and M. Peng, *J. Lumin*., 2012, **132**, 1921.

69 F. Deng and Y. Liu, *J. Lumin*., 2012, **132**, 443.

70 Y. Song, Y. Liu, W. Liu, F. A. Villamena and J. L. Zweier, *RSC Adv*., 2014, **4**, 47649.

71 Y. Y. Yue, X. G. Chen, J. Qin and X. J. Yao, *J. Pharm. Biomed. Anal*., 2009, **49**, 756.

72 (a) F. Samari, M. Shamsipur, B. Hemmateenejad, T. Khayamian and S. Gharaghani, *Eur. J. Med. Chem*., 2012, **54**, 255. (b) N. Shahabadi, M. Maghsudi and S. Rouhani, *Food Chem*., 2012, **135**, 1836.

73 Y. J. Hu, Y. Liu, L. X. Zhang, R. M. Zhao and S. S. Qu, *J. Mol. Struct*., 2005, **750**, 174.

74 W. Y. He, Y. Li, C. X. Xue, Z. D. Hu, X. G. Chen and F. L. Sheng, *Bioorg. Med. Chem*., 2005, **13**, 1837.

75 P. Kalaivani, R. Prabhakaran, F. Dallemer and K. Natarajan, *RSC Adv*., 2014, **4**, 51850.

76 K. Abdi, H. Hadadzadeh, M. Weil and M. Salimi, *Polyhedron*, 2012, **31**, 638.

77 Schrödinger, LLC, Version 1.3, The PyMOL Molecular Graphics System.

78 Y. Zhao and D. G. Truhlar, *J. Phys. Chem*., 2006, **110**, 5121.

79 K. Gkionis, S. T. Mutter and J. A. Platts, *RSC Adv*., 2013, **3**, 4066.

Table 1 Bond lengths and bond angles of the Rh(III) complex in the solid-state (X-ray data), gas phase, water medium, and after its interaction with DNA (computational data).

Bond lengths (Å)	Solid-state	Gas phase	After interaction with DNA in the gas phase	Water medium	After interaction with DNA in water
Rh(1)-C(11)	1.970(10)	2.0085	1.9404	2.0094	1.9398
Rh(1)-C(22)	1.993(10)	2.0085	1.9402	2.0094	1.9213
Rh(1)-N(1)	2.035(9)	2.0775	2.0883	2.0760	2.0545
Rh(1)-N(2)	2.037(9)	2.0774	2.0537	2.0762	2.0596
Rh(1)-N(3)	2.224(7)	2.3284	2.2492	2.3118	2.3419
Rh(1)-N(4)	2.257(7)	2.3278	2.2533	2.3124	2.2351
Bond angles (°)					
N(1)-Rh(1)-C(11)	80.9(5)	81.127	81.692	81.121	82.452
N(2)-Rh(1)-C(22)	79.9(4)	81.128	82.492	81.125	82.576
N(3)-Rh(1)-N(4)	80.1(3)	78.722	79.786	79.018	79.273
N(1)-Rh(1)-N(2)	171.6(3)	174.379	176.147	174.693	175.728
N(4)-Rh(1)-C(11)	171.7(4)	173.491	165.889	173.810	168.701
N(3)-Rh(1)-C(22)	173.4(3)	173.487	172.840	173.858	165.445
N(2)-Rh(1)-N(4)	91.8(3)	87.733	93.257	87.514	86.780
N(3)-Rh(1)-N(1)	87.5(3)	87.731	87.667	87.527	85.240
C(11)-Rh(1)-C(22)	93.9(4)	91.246	98.028	90.792	104.957
N(4)-Rh(1)-C(22)	94.1(3)	95.040	94.594	95.151	86.264
N(1)-Rh(1)-C(22)	96.3(4)	94.909	96.881	95.116	98.363
N(2)-Rh(1)-N(3)	97.1(3)	96.631	93.334	96.583	94.880
N(2)-Rh(1)-C(11)	91.9(4)	94.917	94.617	95.130	93.277
N(4)-Rh(1)-N(1)	95.9(3)	96.622	90.581	96.590	97.431
N(3)-Rh(1)-C(11)	92.1(3)	95.047	88.076	95.098	89.469

Table 2 IC_{50} values (μM) for the compounds towards HepG2, HT-29, and SH-SY5Y cells.

Compound	HepG2	HT-29	SH-SY5Y
$[Rh(phpy\text{-}\kappa^2N,C^{2'})_2(dafone)]ClO_4$	6.46	> 40	29
*Cis*platin	2.40	> 40	29

Table 3 ΔG_b values (kcal mol^{-1}) for the interactions of the Rh(III) complex with DNA and BSA.

	ΔG_b (experimental)	ΔG_b (theoretical)
Complex–DNA	–5.73	–7.5
Complex–BSA	–9.30	–8.3

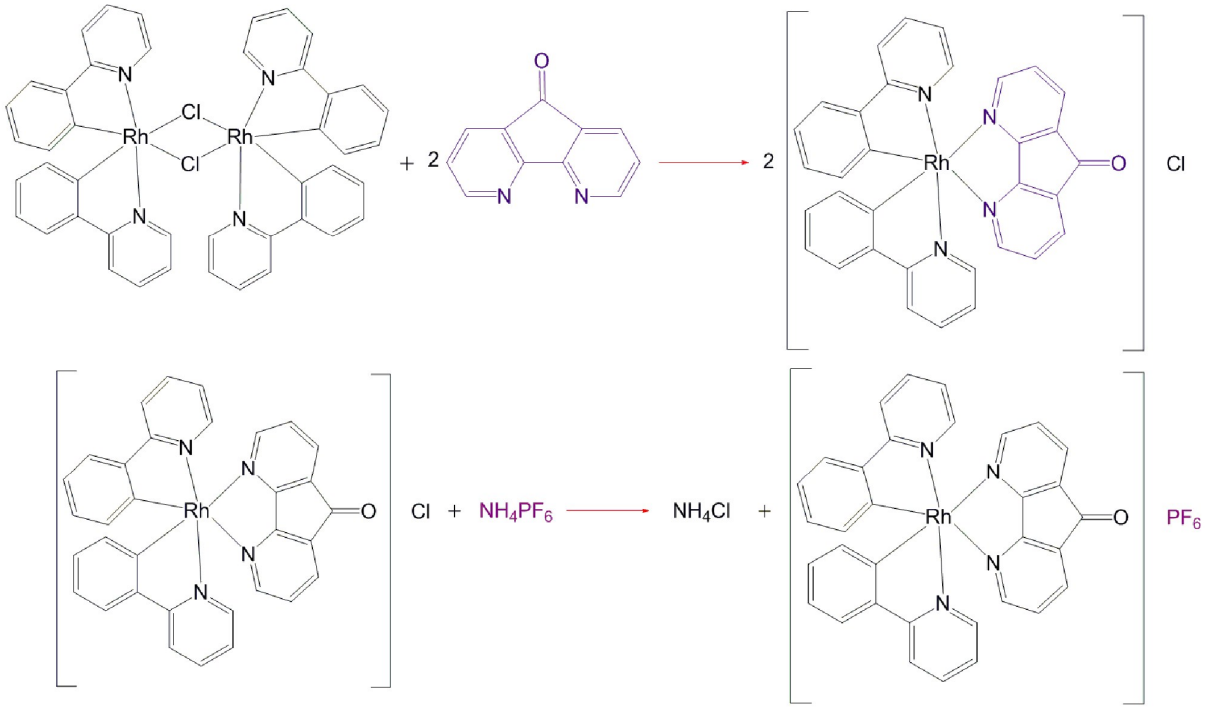

Scheme 1 Synthesis route to [Rh(phpy-$\kappa^2N,C^{2'}$)$_2$(dafone)]PF$_6$.

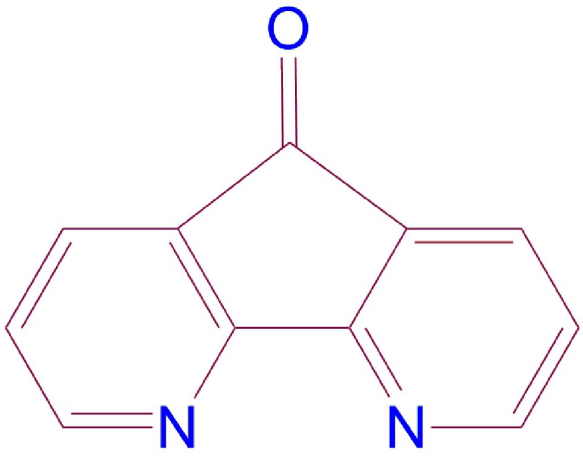

Scheme 2 Molecular structure of dafone.

Figure Captions

Fig. 1 ORTEP drawing of [Rh(phpy-$\kappa^2N,C^{2'}$)$_2$(dafone)]PF_6. The counter ion (PF_6) and water molecule have been omitted for clarity.

Fig. 2 Electronic absorption spectra for the titration of the Rh(III) complex (2×10^{-5} M) with increasing amounts of FS-DNA (0–87.2 μM) in buffer solution (5 mM Tris–HCl/10 mM NaCl at pH 7.2). The arrow shows the changes in the absorbance after DNA addition. Inset: Plot of [DNA]/($\varepsilon_a - \varepsilon_f$) *vs.* [DNA].

Fig. 3 Plot of I_0/I *vs.* [Complex]. Inset: Emission spectra of the EthBr molecule bound to FS-DNA in the absence (0 μM) and presence of increasing amounts of the Rh(III) complex (0.5–8 μM) at room temperature in Tris–HCl/NaCl buffer solution at pH 7.2, λ_{ex} = 520 nm. The arrow shows the intensity changes in increasing concentration of the Rh(III) complex.

Fig. 4 Absorption spectral traces of BSA in Tris–HCl/NaCl buffer upon addition of the Rh(III) complex (0–0.8 μM). The arrows show the intensity changes upon increasing the concentration of the Rh(III) complex.

Fig. 5 The Stern–Volmer plot of the interaction of the Rh(III) complex with BSA after correction for the inner-filter effect. Inset: Fluorescence spectra of BSA (6×10^{-6} M) in the absence (0 μM) and presence of different concentrations of the Rh(III) complex (0.2–2.2 μM). The arrow shows the intensity changes in increasing concentration of the Rh(III) complex.

Fig. 6 The cytotoxic effect of the Rh(III) complex against the HepG2, HT-29, and SH-SY5Y cancer cell lines in a concentration-dependent manner.

Fig. 7 (*a*) Molecular docking of the Rh(III) complex with DNA. (*b*) The bases of DNA with dominant interactions with the complex in the active site.

Fig. 8 Two-dimensional interactions between the Rh(III) complex and DNA generated by LIGPLOT+.

Fig. 9 (*a*) The interaction of the Rh(III) complex with BSA using the Hex docking software. (*b*) The dominant interactions of the residues of BSA with the complex in the active sites.

Fig. 10 Two-dimensional interactions between the Rh(III) complex and BSA generated by LIGPLOT+.

Fig. 11 The optimized structure of (DNA + Rh(III) complex) in the gas phase obtained using the ONIOM calculations.

Fig. 12 The optimized structure of (DNA + Rh(III) complex + water) obtained using the ONIOM calculations.

Fig. 13 The scheme of the equations used for calculating the interaction energy between DNA and the Rh(III) complex in (*a*) the gas phase, and (*b*) water.

Fig. 14 The calculated absorption spectrum of the Rh(III) complex in acetonitrile compared with the corresponding experimental spectrum. The vertical blue lines show the position and intensity of the calculated ionization bands of the complex.

Fig. 15 The calculated molecular orbitals of the Rh(III) complex related to the identified absorption lines with roman numbers in Fig. 14.

Fig. 16 The calculated absorption spectra of the Rh(III) complex with (dotted green line) and without (solid blue line) interaction with DNA in water compared with the corresponding experimental spectra (dotted red line).

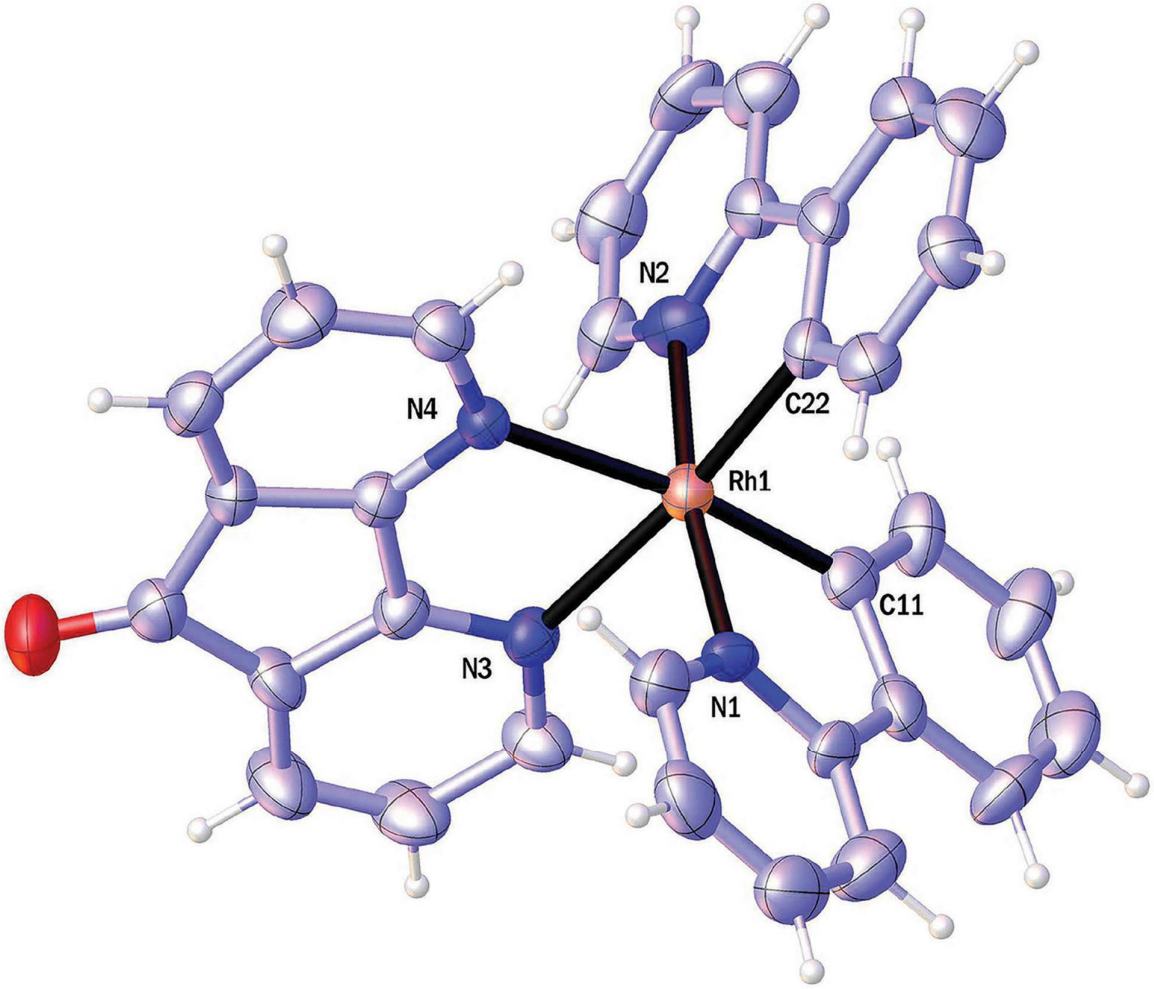

Fig. 1 ORTEP drawing of [Rh(phpy-$\kappa^2N,C^{2'}$)$_2$(dafone)]PF_6. The counter ion (PF_6) and water molecule have been omitted for clarity.

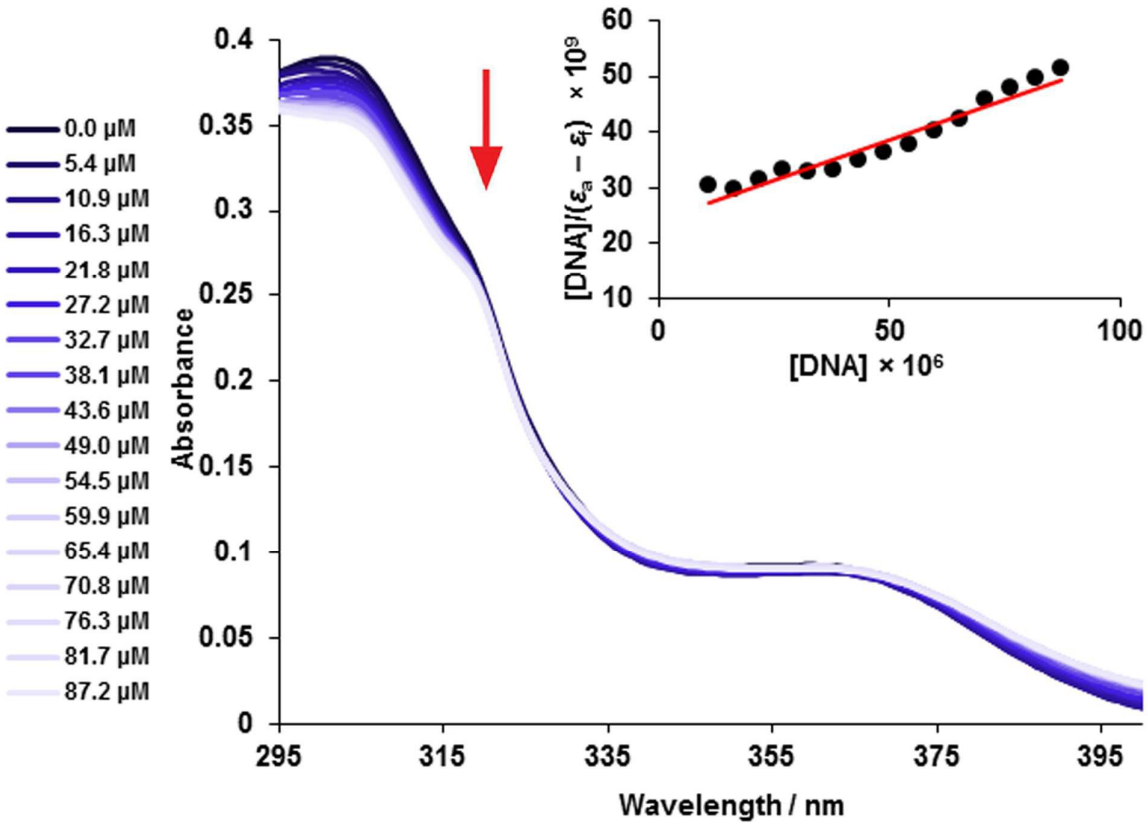

Fig. 2 Electronic absorption spectra for the titration of the Rh(III) complex (2×10^{-5} M) with increasing amounts of FS-DNA (0–87.2 μM) in buffer solution (5 mM Tris–HCl/10 mM NaCl at pH 7.2). The arrow shows the changes in the absorbance after DNA addition. Inset: Plot of [DNA]/($\varepsilon_a - \varepsilon_f$) *vs.* [DNA].

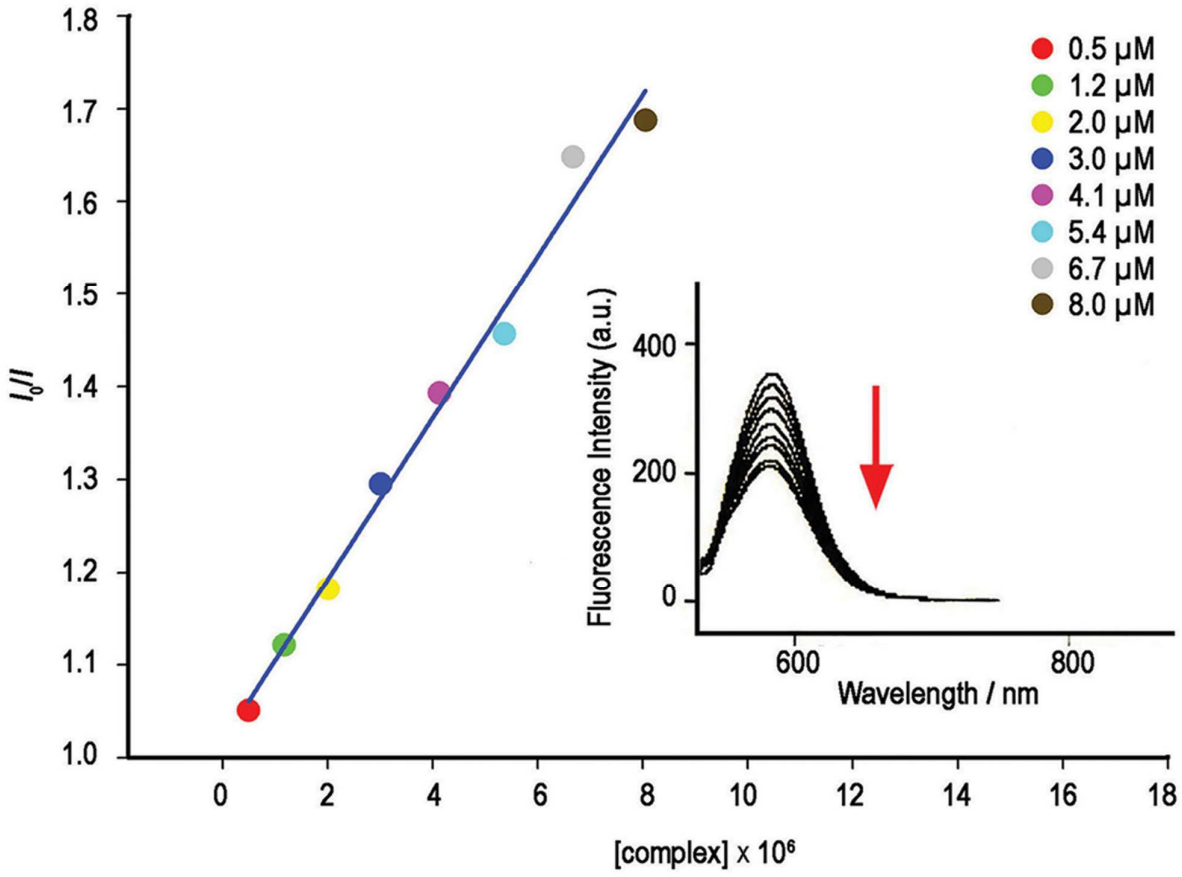

Fig. 3 Plot of I_0/I *vs.* [Complex]. Inset: Emission spectra of the EthBr molecule bound to FS-DNA in the absence (0 μM) and presence of increasing amounts of the Rh(III) complex (0.5–8 μM) at room temperature in Tris–HCl/NaCl buffer solution at pH 7.2, λ_{ex} = 520 nm. The arrow shows the intensity changes in increasing concentration of the Rh(III) complex.

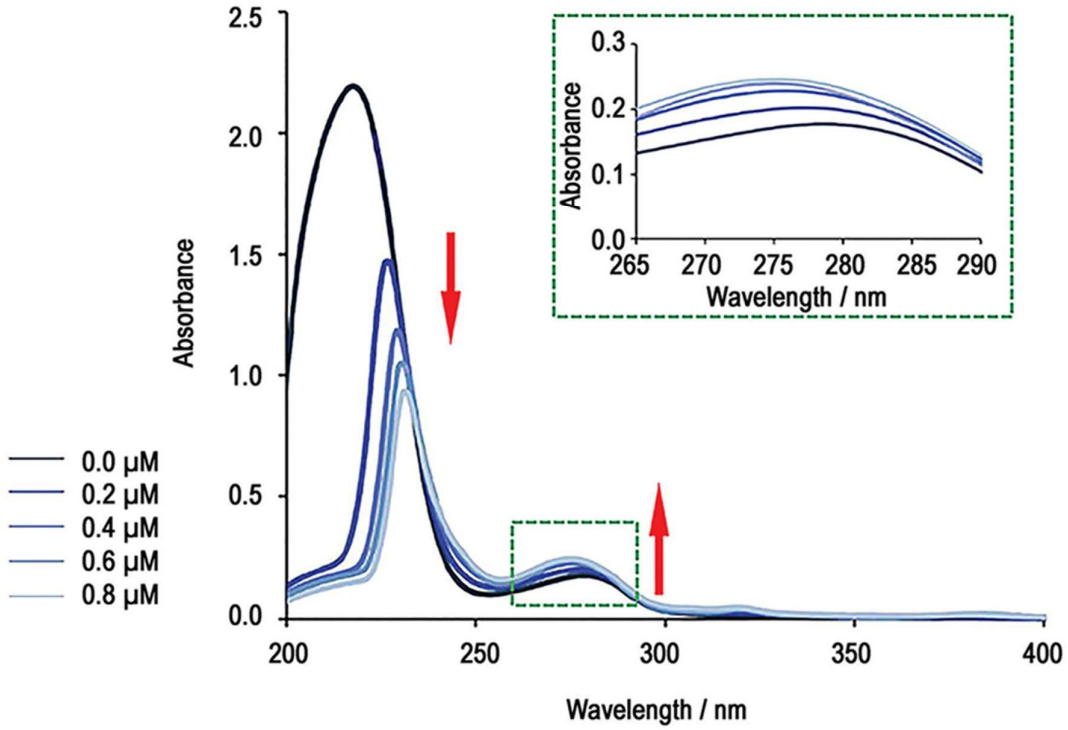

Fig. 4 Absorption spectral traces of BSA in Tris–HCl/NaCl buffer upon addition of the Rh(III) complex (0–0.8 μM). The arrows show the intensity changes upon increasing the concentration of the Rh(III) complex.

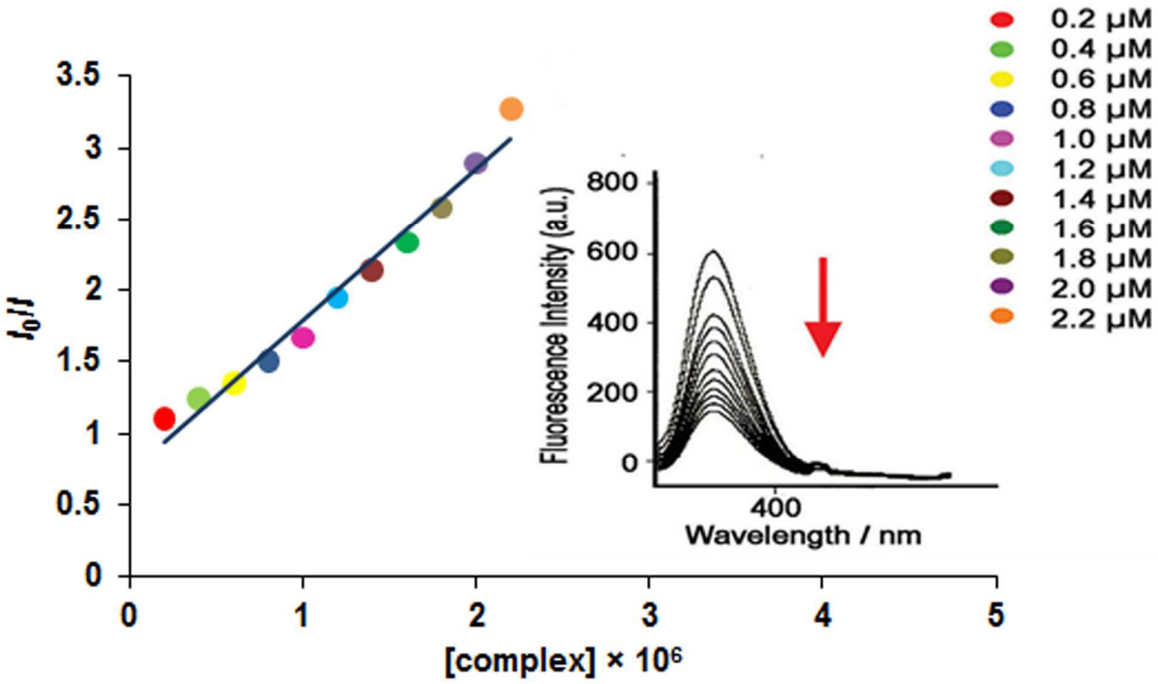

Fig. 5 The Stern–Volmer plot of the interaction of the Rh(III) complex with BSA after correction for the inner-filter effect. Inset: Fluorescence spectra of BSA (6×10^{-6} M) in the absence (0 μM) and presence of different concentrations of the Rh(III) complex (0.2–2.2 μM). The arrow shows the intensity changes in increasing concentration of the Rh(III) complex.

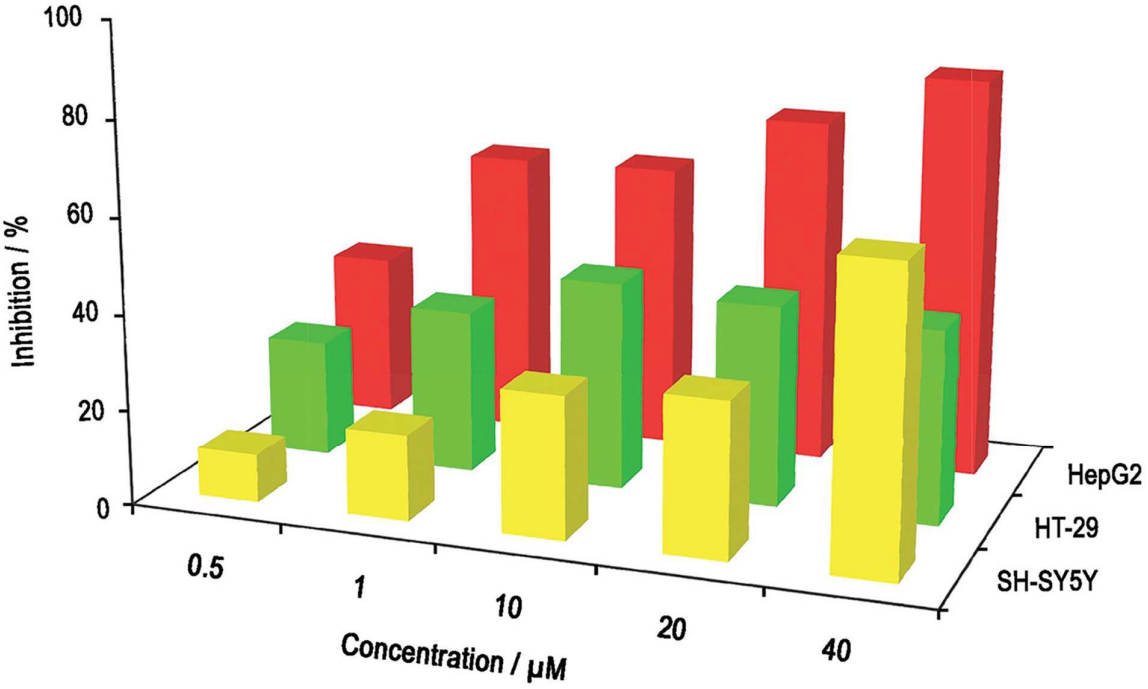

Fig. 6 The cytotoxic effect of the Rh(III) complex against the HepG2, HT-29, and SH-SY5Y cancer cell lines in a concentration-dependent manner.

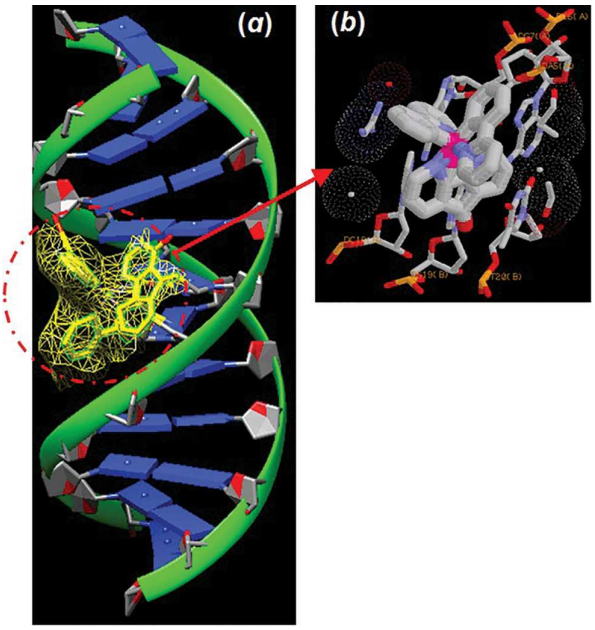

Fig. 7 (*a*) Molecular docking of the Rh(III) complex with DNA. (*b*) The bases of DNA with dominant interactions with the complex in the active site.

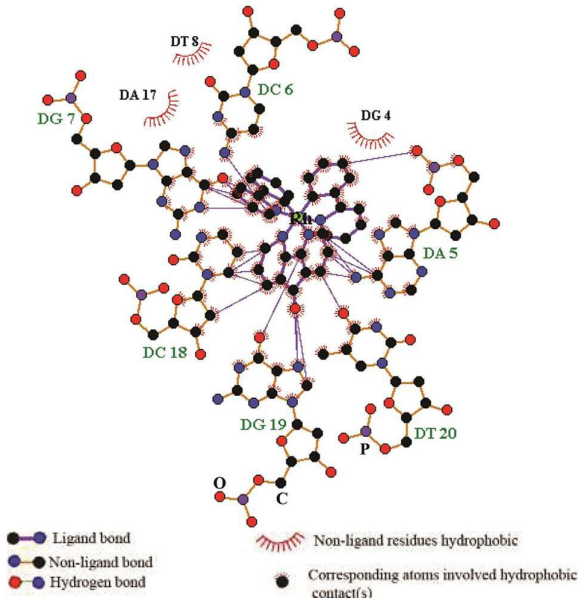

Fig. 8 Two-dimensional interactions between the Rh(III) complex and DNA generated by LIGPLOT+.

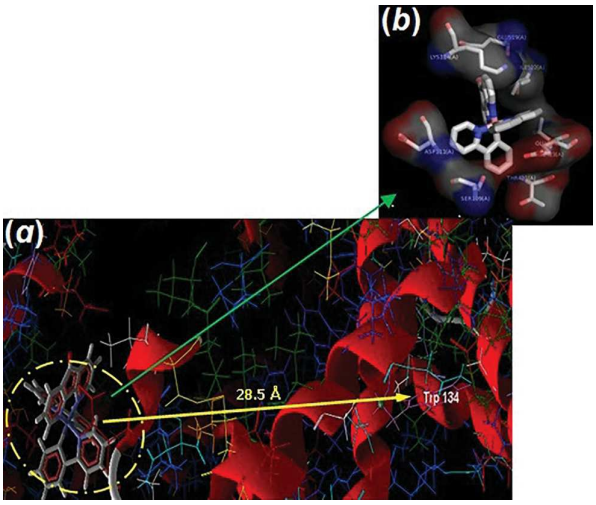

Fig. 9 (*a*) The interaction of the Rh(III) complex with BSA using the Hex docking software. (*b*) The dominant interactions of the residues of BSA with the complex in the active sites.

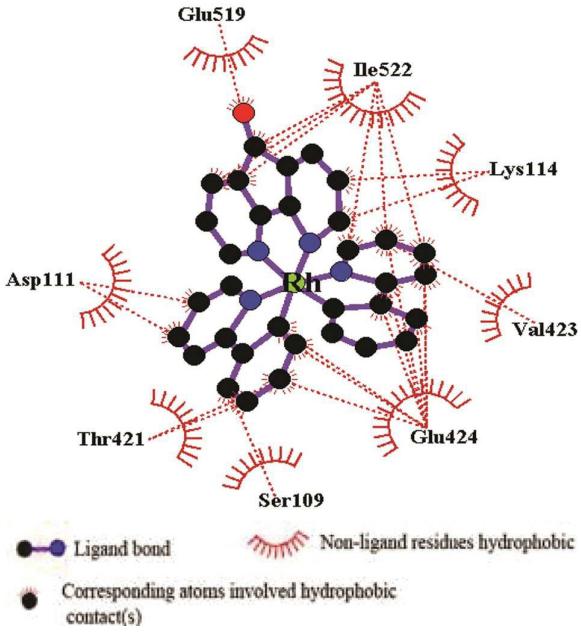

Fig. 10 Two-dimensional interactions between the Rh(III) complex and BSA generated by LIGPLOT+.

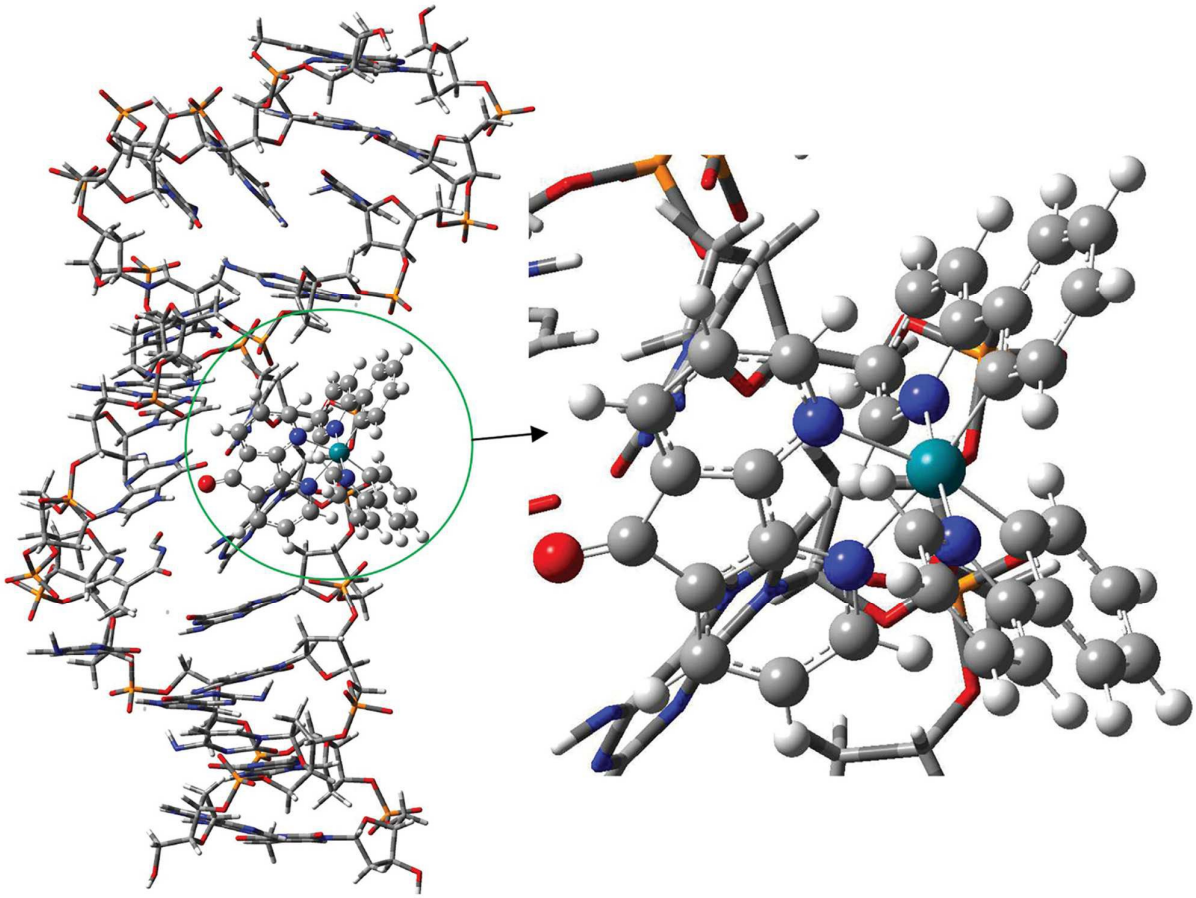

Fig. 11 The optimized structure of (DNA + Rh(III) complex) in the gas phase obtained using the ONIOM calculations.

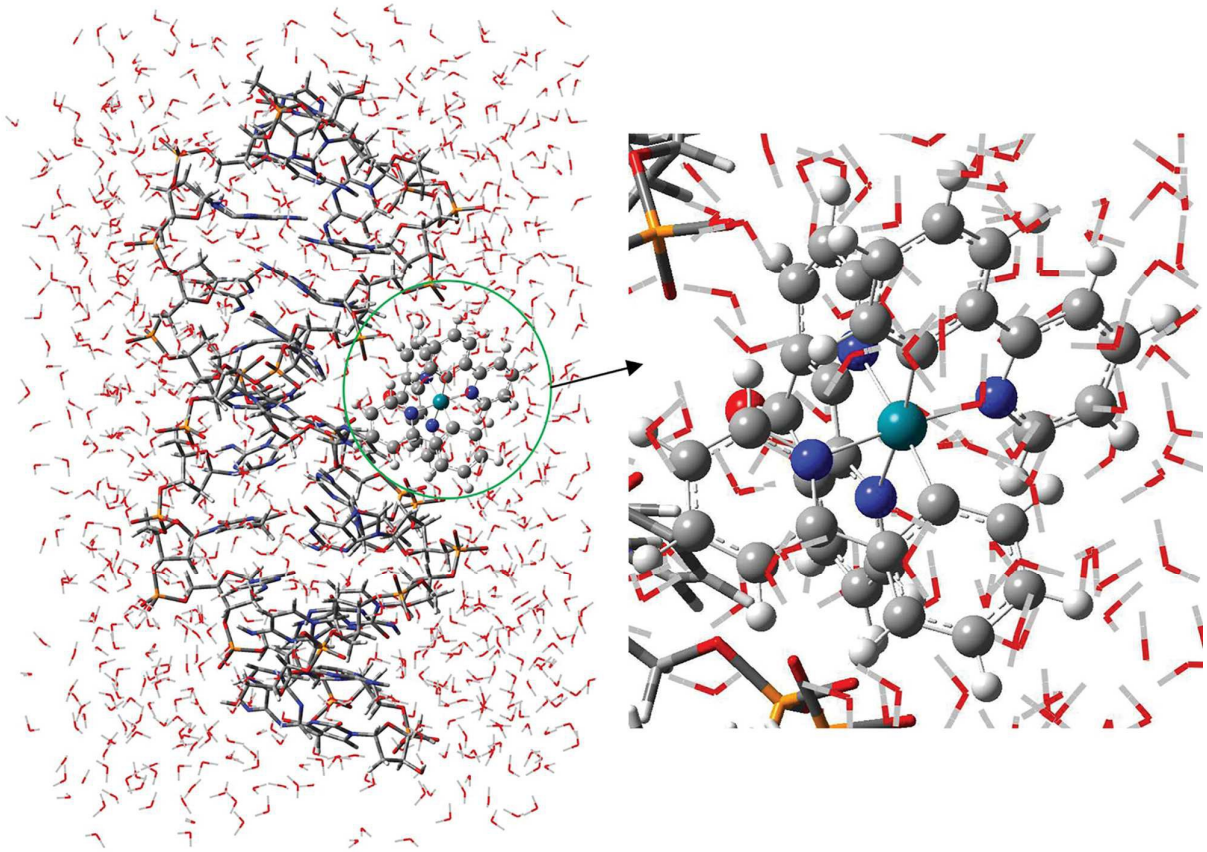

Fig. 12 The optimized structure of (DNA + Rh(III) complex + water) obtained using the ONIOM calculations.

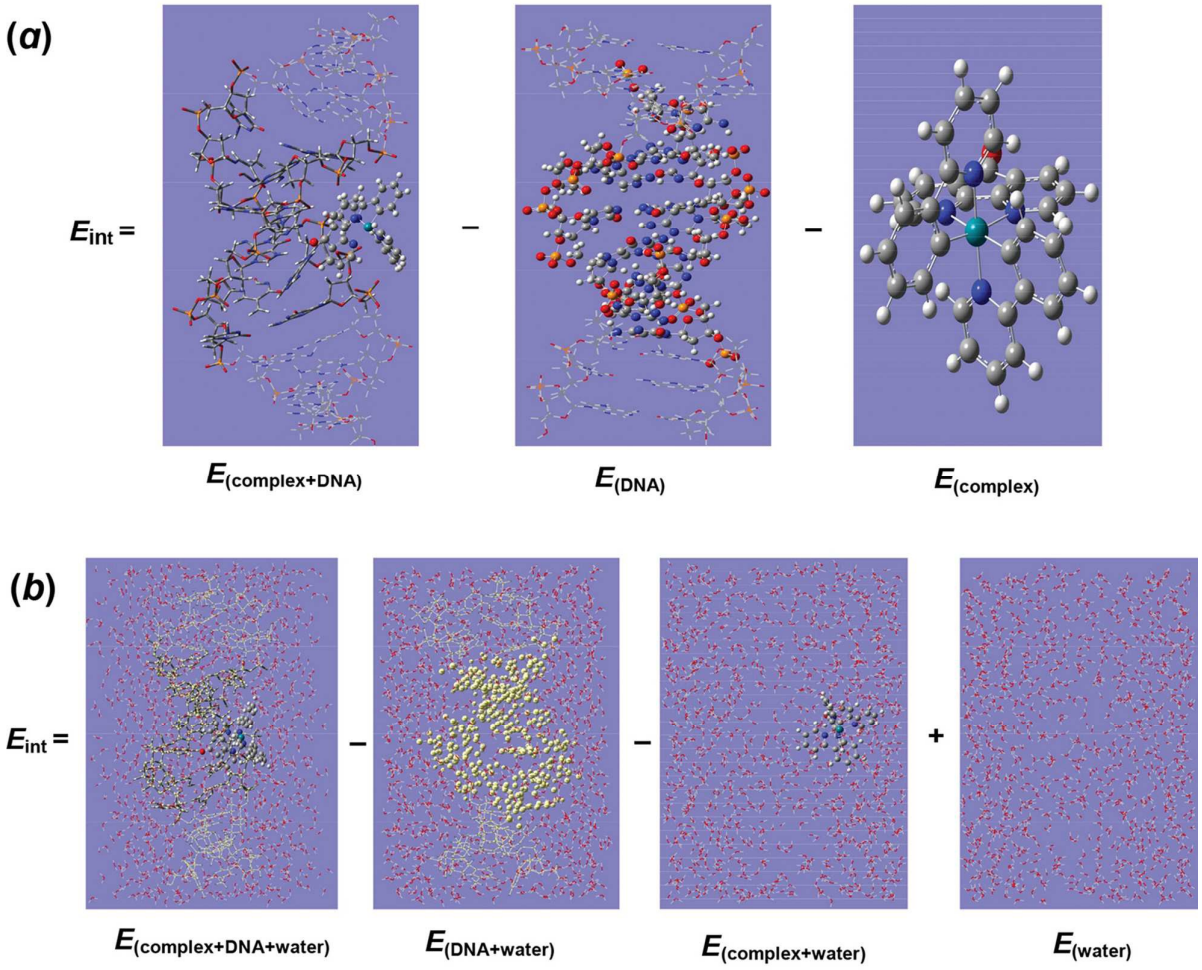

Fig. 13 The scheme of the equations used for calculating the interaction energy between DNA and the Rh(III) complex in (*a*) the gas phase, and (*b*) water.

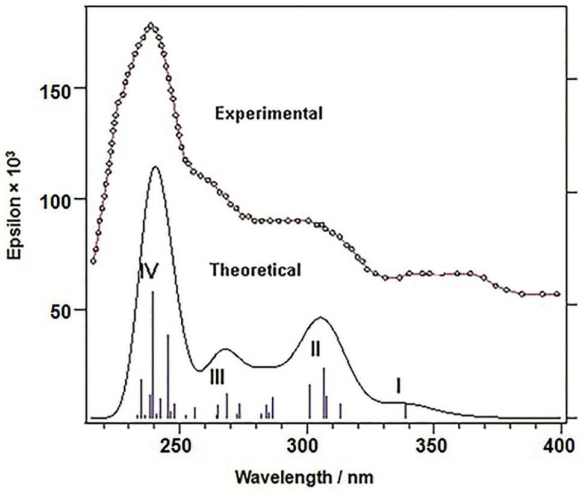

Fig. 14 The calculated absorption spectrum of the Rh(III) complex in acetonitrile compared with the corresponding experimental spectrum. The vertical blue lines show the position and intensity of the calculated ionization bands of the complex.

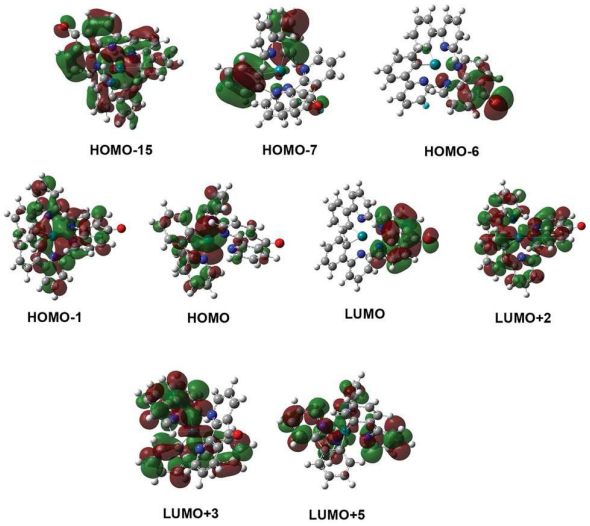

Fig. 15 The calculated molecular orbitals of the Rh(III) complex related to the identified absorption lines with roman numbers in Fig. 14.

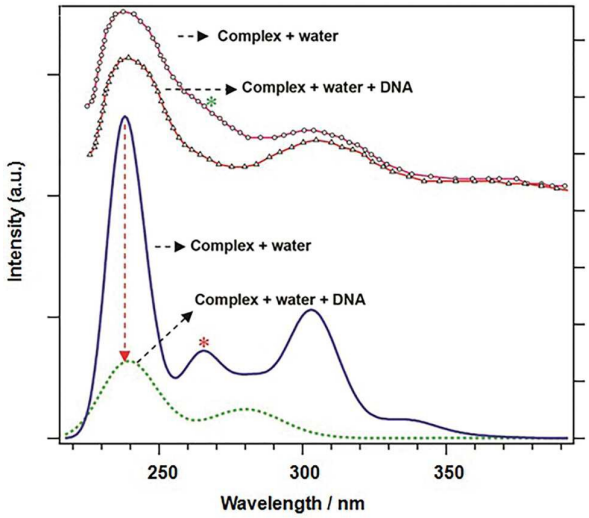

Fig. 16 The calculated absorption spectra of the Rh(III) complex with (dotted green line) and without (solid blue line) interaction with DNA in water compared with the corresponding experimental spectra (dotted red line).

"For Table of Contents Only"

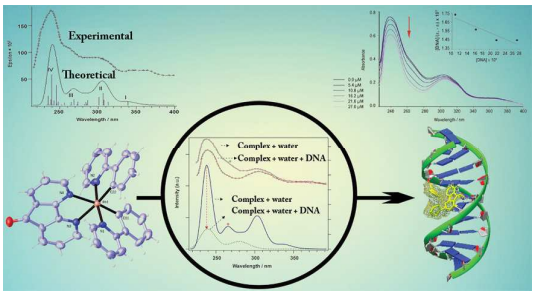

The interaction of a new cyclometallated Rh(III) complex, $[Rh(phpy\text{-}\kappa^2N,C^{2'})_2(dafone)]^+$, with DNA and BSA was investigated. The three-layer ONIOM method (QM:QM:MM) was employed to calculate the interaction energy between DNA and the complex. The calculations confirm the variations observed in the spectra of the complex due to its interaction with DNA.